5

General Topics in Passive Gamma-Ray Assay

J. L. Parker

This chapter discusses general topics that apply to the gamma-ray assay techniques discussed in Chapters 7 to 10. All these topics must be understood if optimum results are to be obtained from any assay technique. The topics include

- Energy calibration and determination of peak position
- Energy resolution measurements
- Determination of full-energy-peak area
- Rate-related losses and corrections
- Effects of the inverse-square law
- Detector efficiency measurements.

5.1 ENERGY CALIBRATION AND DETERMINATION OF PEAK POSITION

5.1.1 Introduction

The energy calibration of a gamma-ray spectroscopy system is the relationship between the energy deposited in the detector by a gamma ray and the amplitude of the corresponding amplifier output pulse. The pulse amplitude is measured by the analog-to-digital converter (ADC) of a multichannel analyzer (MCA) or by one or more single-channel analyzers (SCAs). The energy calibration is used to determine the width and location of regions of interest (ROIs), to determine resolution, and to find the energies of any unrecognized gamma rays.

The energy calibration of a good spectroscopy system is nearly linear:

$$E = mx + b \tag{5-1}$$

where E = energy deposited in detector
       m = slope
       x = amplitude of output pulse
       b = intercept.

The assumption of linearity is usually sufficient for nondestructive assay (NDA) techniques. However, no system is exactly linear; each has small but measurable nonlinearities. When a more accurate relationship is necessary, a higher order polynomial is used. Gamma-ray energies can be determined to within 0.01 to 0.05 keV using a nonlinear calibration curve and several standard gamma-ray sources with energies known to better than 0.001 keV.

Low-resolution detectors [for example, NaI(Tl) scintillators] often use Equation 5-1 with a zero intercept (b = 0). The linear approximation is usually good enough for even high-resolution NDA applications. For a good germanium detector, a linear calibration will determine the peak energy to within a tenth of a keV, which is adequate to identify the isotopes present in the measured sample. For most of the isotopes of interest to NDA, the pattern of the gamma-ray spectrum is so distinctive that a visual examination of the MCA display by an experienced person is sufficient to identify the isotopes present. Figure 5.1 shows the characteristic spectrum of low-burnup plutonium, and Figure 5.2 shows the characteristic spectrum of natural uranium (0.7% ^{235}U).

The calibration procedure involves determining the channel location of peaks of known energy and fitting them to the desired calibration function. Often, the gamma rays from the measured nuclear material sample can be used to determine the energy calibration. Figure 5.1 shows that plutonium spectra have interference-free peaks at 59.54, 129.29, 148.57, 164.57, 208.00, 267.54, 345.01, 375.04, and 413.71 keV. Similar internal calibrations are possible for many isotopes (Refs. 1 and 2).

When the measured nuclear material cannot provide an adequate calibration, isotopic standards are used that emit gamma rays of known energies. Table 5-1 lists some of the most frequently used isotopes with the half-lives and energies of their principal emissions (Ref. 3). Most of the isotopes listed emit only a few gamma rays and are useful with both low- and high-resolution detectors. All the isotopes listed in the table are available from commercial vendors. Packaged sources usually contain a single isotope and are produced in a wide variety of geometries. Source strengths between 0.1 and 100 μCi are usually adequate for energy calibration. Convenient sets of six to eight single-isotope sources are available from most vendors. Their use is required for setting up, testing, and checking many performance parameters of spectroscopy systems. The source sets are useful for determining energy calibration, testing detector resolution, measuring detector efficiency, setting the pole-zero adjustment, and correcting for rate-related counting losses.
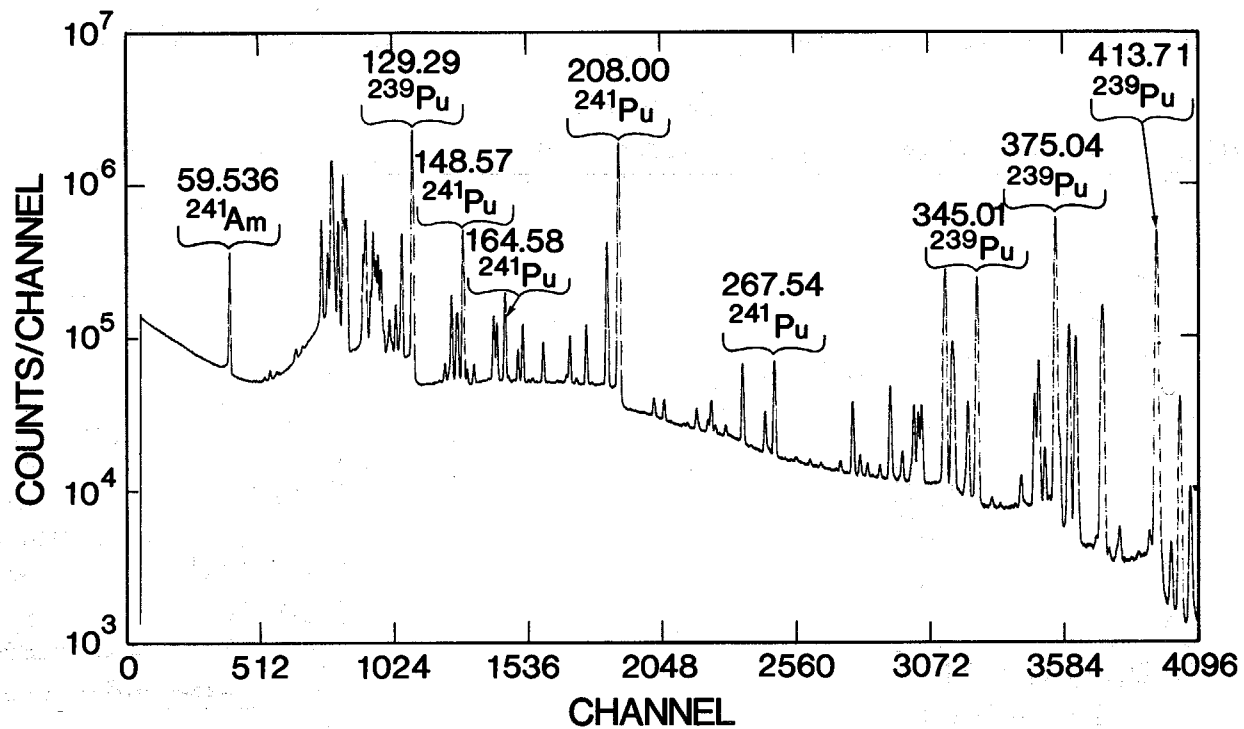
Fig. 5.1 A high-resolution spectrum of low-burnup plutonium. The indicated peaks are useful in the energy calibration of plutonium spectra. The energy in keV is equal to the channel number divided by 10, plus 20.
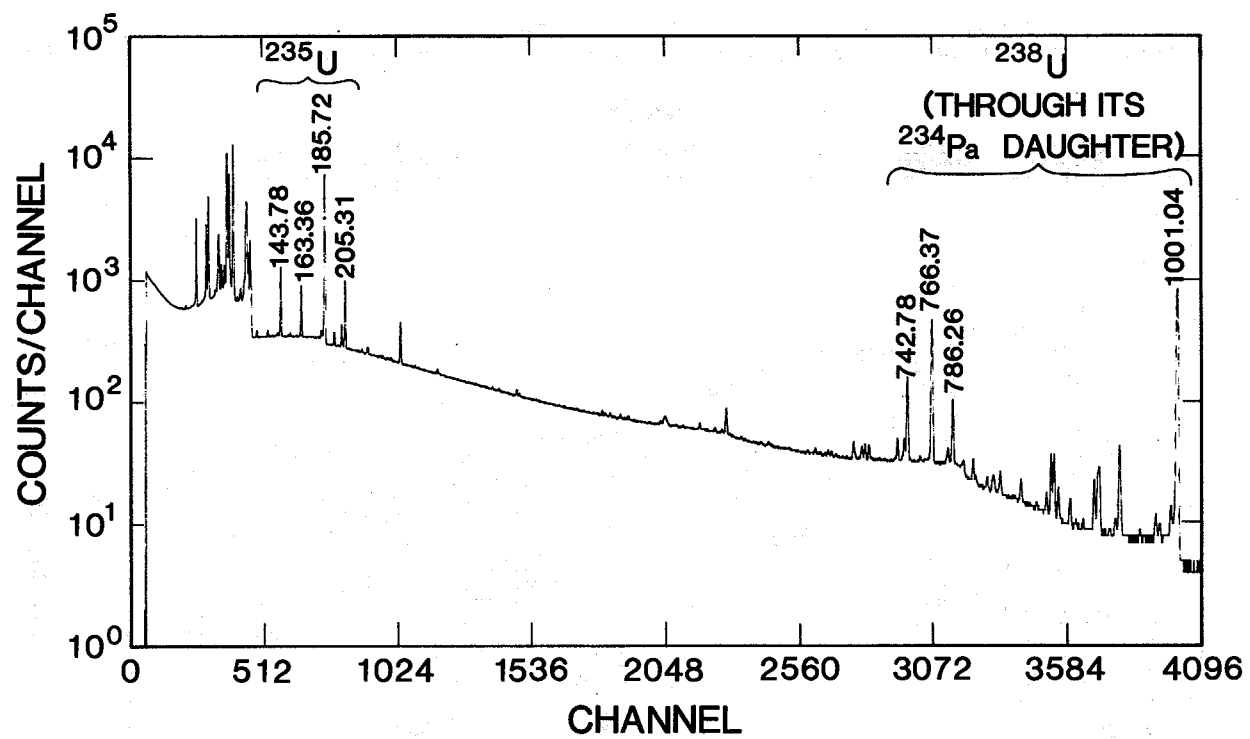
Fig. 5.2 A high-resolution spectrum of natural uranium (0.7% ^{235}U). The energy in keV is equal to the channel number divided by 4.

Table 5-1. Half-lives and energies of major emissions for selected isotopes[a]

Isotopes	Half-Life	Energy (keV)	Remarks
[241]Am	433 yr	59.54	Many others, but weaker by factors 10^4 or greater
[137]Cs	29.9 yr	661.64	The only other emission is from Ba K x rays
[133]Ba	10.9 yr	81.0, 276.40, 302.85, 356.00, 383.85	Several others, but much weaker
[60]Co	5.3 yr	1173.23, 1332.51	
[22]Na	2.8 yr	511.01 1274.51	Annihilation radiation
[55]Fe	2.7 yr	Mn K x rays 5.9, 6.5	Often used for low-energy calibration
[109]Cd	1.2 yr	88.04	Ag K x rays at 22.16 keV and 24.9 keV
[54]Mn	312 d	834.8	Monoenergetic source
[65]Zn	244 d	511.01 1115.5	Annihilation radiation
[57]Co	271 d	122.06, 136.47	Two others of higher energy, but much weaker
[75]Se	120 d	121.12, 136.00, 264.65, 279.53, 400.65	Several others, but much weaker

[a]Listed in decreasing order of half-life. All isotopes listed should be useful for at least 1 yr, because the half-lives are greater than 100 days.

Gamma-ray standards are available with several isotopes in one capsule. These multienergy sources are used to define the energy calibration curve and efficiency curve of high-resolution detectors. The National Bureau of Standards (NBS) source SRM-4275 contains [125]Sb (2.75-yr half-life), [154]Eu (8.49-yr half-life), and [155]Eu (4.73-yr half-life) and emits 18 well-resolved gamma rays between 27 and 1275 keV. The emission rates of all 18 certified gamma rays are known to better than 1%.

5.1.2 Linear Energy Calibration

Equation 5-1 describes the assumed functional form for a linear energy calibration. If the positions x_1 and x_2 of two full-energy peaks of energies E_1 and E_2 are known, m and b can be computed from

$$m = \frac{(E_2 - E_1)}{(x_2 - x_1)} \tag{5-2}$$

$$b = \frac{(x_2 E_1 - x_1 E_2)}{(x_2 - x_1)} . \tag{5-3}$$

For a two-point calibration, the two calibration peaks should be near the low- and high-energy ends of the energy range of interest to avoid long extrapolations beyond the calibrated region.

Often, when an unacceptable degree of nonlinearity exists, several linear calibrations can be used over shorter energy intervals. The high-resolution spectrum of most plutonium samples has nine well-resolved peaks between 59.5 keV and 413.7 keV so that eight linear calibrations can be constructed for the intervals between adjacent peaks; none of the intervals is greater than 78 keV. A series of short linear calibrations can often be as accurate as a single quadratic or higher-order calibration curve.

When more than two peaks span the energy range of interest, least-squares fitting techniques can be used to fit a line to all the peaks. This method can be used to obtain the following expressions for m and b for n peaks:

$$m = \frac{n \sum x_i E_i - \sum x_i \sum E_i}{\Delta} \tag{5-4}$$

$$b = \frac{\sum x_i^2 \sum E_i - \sum x_i \sum x_i E_i}{\Delta} \tag{5-5}$$

where $\Delta = n \sum x_i^2 - \left(\sum x_i \right)^2$.

Most hand calculators can perform a linear least-squares fit. Many MCA systems can determine the x_i and compute m and b for any selected number of peaks. Some systems will also do a quadratic fit.

A linear energy calibration is usually adequate for NDA applications. Table 5-2 gives the results of two-point and nine-point linear calibrations of a high-quality plutonum spectrum. The nominal calibration, E (keV) = 0.1x + 20.0, was established by stabilizing the 59.536-keV gamma ray of [241]Am at channel 395.0 and the 413.712-keV gamma ray of [239]Pu at channel 3937.0. The second column of Table 5-2 gives the peak positions determined by fitting a Gaussian curve to the upper portion of the peaks. The third and fourth columns give the difference between the accepted energies and those obtained from the two-point and nine-point calibrations. Although there is a measurable curvature to the energy versus channel relation, the maximum error is only ~0.03 keV for the two-point calibration and ~0.017 keV for the nine-point calibration. The consistency of the results in Table 5-2 indicates that the peak positions have been located to within ~0.1 channel (~0.01 keV) and that the accepted energy values are consistent within ~0.01 keV.

Table 5-2. Results of linear energy calibrations of a high-quality plutonium spectrum

Accepted Energies (keV)	Peak Positions (channels)	Energy Difference (keV)[a]	
		Two-Point Calibration	Nine-Point Calibration
59.536	395.00	- - -	− 0.017
129.294	1092.77	0.014	− 0.001
148.567	1285.51	0.014	0.000
164.58	1445.80	0.029	+ 0.015
208.000	1879.96	0.022	+ 0.009
267.54	2475.37	0.019	+ 0.007
345.014	3249.98	0.001	− 0.009
375.042	3550.40	0.013	+ 0.004
413.712	3937.00	- - -	− 0.008

[a]The tabulated numbers are the energies from the calibration minus the accepted energies. For the two-point calibration, m = 0.099993 keV/channel and b = 20.039 keV. For the nine-point calibration, m = 0.099996 keV/channel and b = 20.021 keV.

5.1.3 Determination of Peak Position (Centroid)

Even with high-resolution detectors, full-energy peaks are usually at least several channels wide. The peaks are nearly symmetric, and the peak positions are chosen as the peak centers defined by the axis of symmetry. Full-energy peaks are usually well described by a Gaussian function of the form

$$y(x) = y_0 \exp\left[- (x - x_0)^2 / 2\sigma^2 \right] \qquad (5\text{-}6)$$

where y(x) = number of counts in channel x
    y_0 = peak amplitude
    x_0 = peak centroid
    σ^2 = variance.

References 4, 5, and 6 provide a detailed explanation of the properties of the Gaussian function. The function is symmetric about x_0, which is the peak centroid used in energy calibration. The parameter y_0 is the maximum value of the function and is nearly equal to the maximum counts per channel in the peak if the background under the peak is negligible. The parameter σ^2 (the variance) is related to the full width at half maximum (FWHM) of the function by

$$\text{FWHM} = 2\sqrt{2 \ln 2}\, \sigma = 2.35482\sigma \ . \tag{5-7}$$

The area under the Gaussian curve is given by

$$A = \sqrt{2\pi}\, \sigma y_0 = 2.507\sigma y_0$$
$$= 1.0645(\text{FWHM})y_0 \ . \tag{5-8}$$

The constant in the second form of Equation 5-8 is close to 1.0 because the area of a Gaussian is just a little greater than the area of an isosceles triangle with the same height and width at the half-maximum level.

Full-energy peaks are not exactly Gaussian shaped. For high-quality germanium detectors the deviations are hardly visible, but for lower quality detectors the deviations are easily seen as an excess of counts on the low-energy side of the peak (called tailing). At very high rates or with poorly adjusted equipment, high-energy tailing is sometimes visible. The upper one-half to two-thirds of a peak is usually Gaussian, and the centroid determined by fitting a Gaussian to the upper portion of the peak is a well-defined measure of peak position. Figures 5.3(a), (b), and (c) show the 1332.5-keV full-energy peak of ^{60}Co and the fitted Gaussian function. Figure 5.3(a) is from a high-quality germanium detector at low count rate, with properly adjusted electronics. The deviations from the curve are hardly visible except for a very slight low-energy tailing. Figure 5.3(b) is from a detector with poor peak shape. The low-energy tailing is obvious. Figure 5.3(c) is from the same detector as Figure 5.3(a) but at very high rates that cause distinct high-energy tailing and significant deviation from a true Gaussian shape. In all three situations, the Gaussian function fitted to the upper two-thirds of the peak gives a good peak location.
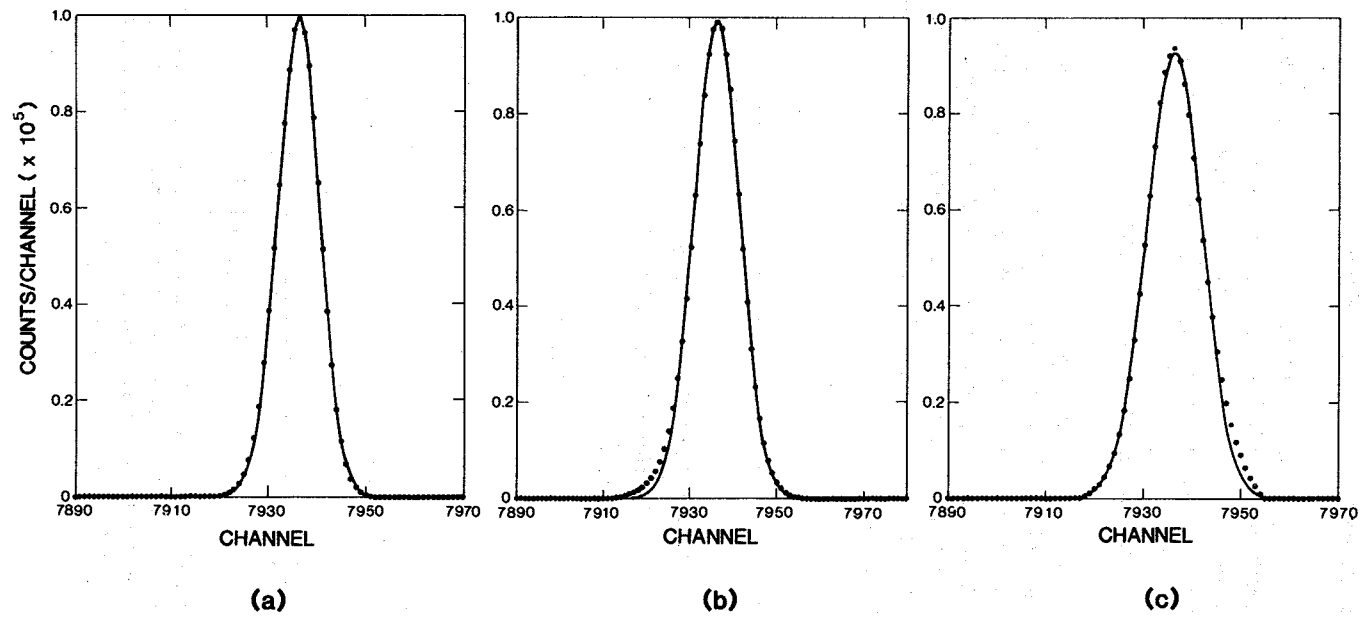
Fig. 5.3 *The 1332.5-keV full-energy peak of ^{60}Co for three combinations of detector and count rate: (a) high-quality germanium detector and low count rate; (b) a germanium detector with poor peak shape; (c) high-quality germanium detector and high count rate. The Gaussian is fitted to the upper two-thirds of the peak.*

5.1.4 Visual Determination of Peak Position

The human eye is very good at bisecting symmetric shapes. When a peak can be spread out sufficiently on the MCA display, estimates of peak positions can often be made to a few tenths of a channel by visual examination. The movable markers (cursors) that are part of most MCA displays help in making visual determinations.

5.1.5 Graphical Determination of Peak Position

Figure 5.4 shows an SCA-acquired spectrum of ^{137}Cs from a high-quality 7.62- by 7.62-cm NaI(Tl) scintillator. It is desirable to plot such spectra as histograms with the width of the bar equal to the window width and the low-energy side of the bar beginning at the threshold voltage setting. Usually the intervals between threshold settings equal the window width. The peak center is determined by drawing a straight line along both sides of the peak through the centers of the bars. The intersection of the two lines is the peak center.
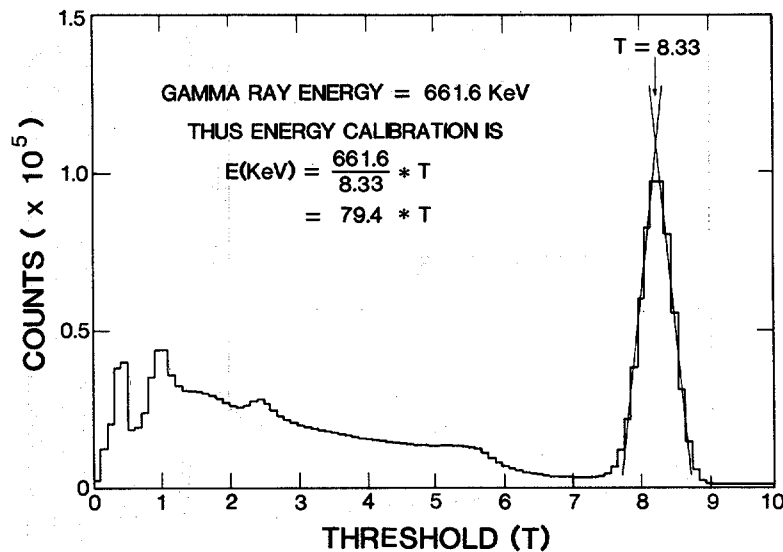
Fig. 5.4 *Plot of an SCA-generated spectrum of ^{137}Cs from a 7.62-cm by 7.62-cm NaI(Tl) scintillation detector. The plot shows how visually fitting the intersection of lines along the sides of the peak is a consistent way of estimating the peak center.*

5.1.6 Determination of Peak Position by the First-Moment Method

The centroid of a positive function y(x) is given by

$$\bar{x} = \frac{\int_{x_1}^{x_2} x\, y(x)\, dx}{\int_{x_1}^{x_2} y(x)\, dx} \approx \frac{\sum x_i y_i}{\sum y_i} \tag{5-9}$$

where x_1 and x_2 are the bounds of the area considered and y_i is the number of counts in channel x_i. This is called the first-moment method because the numerator of Equation 5-9 is the first moment of y(x). For the Gaussian function (Equation 5-6), $\bar{x} = x_0$. For calculational purposes the integrals are replaced by sums that closely approximate them. The Gaussian function only approaches zero as $x \rightarrow \pm\infty$; however, summing over a region approximately three times FWHM is usually adequate. If the peak is symmetric and if the summed region is symmetric about the peak, good results are obtained even without subtracting the background from under the peak. If a large background continuum lies under the peak and an asymmetrically placed summing region is used, the result will be in error. If the underlying continuum is subtracted, the error in calculated peak location caused by an asymmetric summing region is small. Figure 5.5 shows both a good choice and a poor choice of summing regions. Methods for continuum subtraction are discussed later in this chapter.

The first-moment method is particularly useful for peaks with relatively few counts per channel. It should be used with caution on peaks with distinct asymmetry because the calculated centroid will not coincide with the centroid of the Gaussian portion of the peak that must be determined for the energy calibration. Use of the first-moment procedure does not require that the peak have a Gaussian shape, but only that the peak is symmetric.

5.1.7 Determination of Peak Position by the Five-Channel Method

The five-channel method uses the maximum count channel and two adjacent channels on each side to estimate the peak centroid. The relevant formula is

$$x_0 = x_m + \frac{y_{m+1}\,(y_m - y_{m-2}) - y_{m-1}\,(y_m - y_{m+2})}{y_{m+1}\,(y_m - y_{m-2}) + y_{m-1}\,(y_m - y_{m+2})} \tag{5-10}$$

where the subscript m refers to the maximum count channel, and y_i refers to the counts in channel x_i.

Equation 5-10 assumes a Gaussian peak shape. Similar formulas can be derived assuming a parabolic shape at the top of the peak. Equation 5-10 works well when there are 6 to 30 channels above the FWHM point and enough counts in the five channels to clearly delineate the shape of the top of the peak. The five-channel method does not work as well as the first-moment method on broad peaks with poor precision. However, the five-channel method is less sensitive than the first-moment method to asymmetric peak tails from a poor detector.
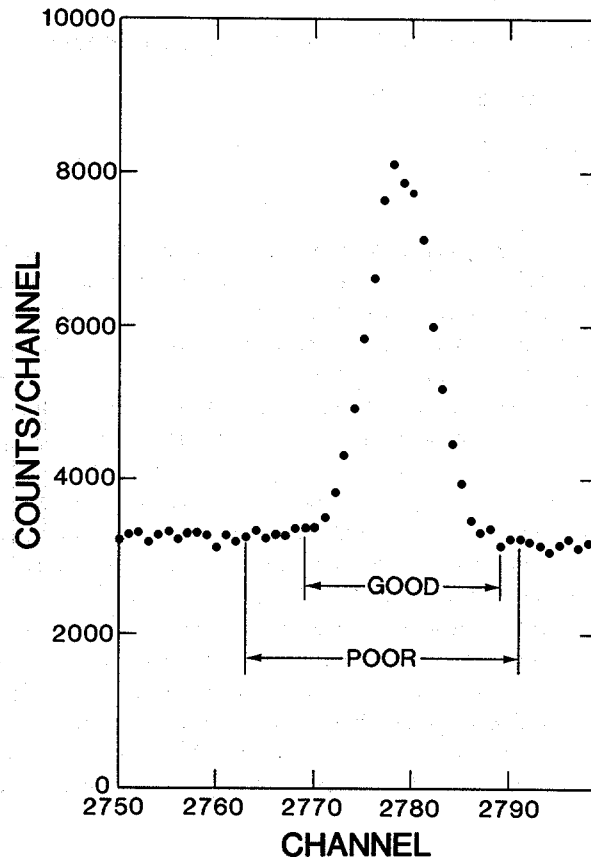
Fig. 5.5 *A spectral peak showing good and poor choices*
of summing regions when determining the peak
centroid by the first-moment method.

5.1.8 Determination of Peak Position by a Linearized Gaussian Fit

This procedure transforms the Gaussian-shaped peak into a line and then fits a line to the transformed peak. The slope and intercept of the fitted line are related to x_0 and σ. The background continuum under the peak is first subtracted so that the fit is made only to the Gaussian-shaped peak.

Transformations that linearize the Gaussian function have been applied only recently to determine the parameters of gamma-ray peaks (Ref. 7). The simplest of a class of similar transformations is the function

$$Q(x) = \ln \frac{y(x-1)}{y(x+1)} = \frac{2}{\sigma^2} x - \frac{2x_0}{\sigma^2} \qquad (5\text{-}11)$$

where y(x) is the number of counts in channel x. The last expression in Equation 5-11 is correct if y(x) is the usual Gaussian function. The linear function Q(x) has a slope m and intercept b given by

$$m = 2/\sigma^2$$

$$b = -2x_0/\sigma^2. \tag{5-12}$$

Solving for σ^2 and x_0 gives

$$\sigma^2 = 2/m$$

$$x_0 = -b/m . \tag{5-13}$$

Equation 5-14 gives the expressions for the slope m and the intercept b of the line fit to the set of points [x, Q(x)] by the weighted-least-squares method:

$$b = \frac{1}{\Delta}\left(\sum \frac{x_i^2}{s_i^2} \sum \frac{Q_i}{s_i^2} - \sum \frac{x_i}{s_i^2} \sum \frac{x_i Q_i}{s_i^2} \right)$$

$$m = \frac{1}{\Delta}\left(\sum \frac{1}{s_i^2} \sum \frac{x_i Q_i}{s_i^2} - \sum \frac{x_i}{s_i^2} \sum \frac{Q_i}{s_i^2} \right) \tag{5-14}$$

where

$$\Delta = \sum \frac{1}{s_i^2} \sum \frac{x_i^2}{s_i^2} - \left(\sum \frac{x_i}{s_i^2} \right)^2$$

s_i^2 = estimated variance of Q(x).

The estimated variance of Q(x) is a function only of the uncertainties in y(x):

$$s^2[Q(x)] = s_r^2[y(x-1)] + s_r^2[y(x+1)] \tag{5-15}$$

where $s_r(y) \equiv s(y)/y$.

If the background continuum is small enough to ignore, then

$$s_r^2[y(x)] \approx 1/y(x) . \tag{5-16}$$

If the background continuum is subtracted by the straight-line procedure later shown in Section 5.3.3, the expression for $s^2[y(x)]$ is given by

$$s^2[y(x)] = y_t(x) + \frac{1}{4}\left[k^2\frac{B_h}{N_h^2} + (2-k)^2\frac{B_l}{N_\ell^2}\right]$$ (5-17)

where $\quad k = \dfrac{2(x - x_\ell)}{(x_h - x_\ell)}$.

Also, $y_t(x)$ is the total counts in channel x and the meanings of the other parameters are given in Section 5.3.3.

For a linear fit there are simple expressions for the estimated variance s^2 of m and b:

$$s^2(m) \simeq \frac{1}{\Delta}\sum\frac{1}{s_i^2}$$

(5-18)

$$s^2(b) \simeq \frac{1}{\Delta}\sum\frac{x_i}{s_i^2}\ .$$

Although the fitting procedure just described may seem somewhat complex, the fit can be performed by a short computer program in only a few seconds. The Gaussian function should be fit to the top three-fourths to two-thirds of the peak to avoid problems with non-Gaussian tails and imprecise data. The n channels in the peak give $n - 2$ values of $Q(x)$. When at least four or five values of $Q(x)$ are used in the fit, the results are more than adequate to determine the peak centroids needed for the energy calibration. Unfortunately, it is very difficult to estimate the statistical uncertainty in x_0 using this fitting procedure. However, experience indicates that for peaks of reasonable precision, the values of x_0 are good to ~ 0.1 channel or better.

In automated operations, a test should be made to determine whether a Gaussian function adequately describes the input data. The reduced chi-square statistic χ^2/ν provides such a test. For the linear fit of $Q(x)$ versus x,

$$\chi^2/\nu = \frac{1}{n-2}\left\{\sum\frac{1}{s_i^2}\left[Q_i - (mx_i + b)\right]^2\right\}$$ (5-19)

where m and b are computed from Equation 5-14 and n is the number of values of $Q(x)$ in the fit. For good fits, χ^2/ν should be ~ 1.00. (See Ref. 5 for a very readable discussion of the properties of χ^2/ν.) For low-precision peaks (up to $\sim 10\ 000$ counts/channel), χ^2/ν is really ~ 1.00 for peaks of qualitatively good shape. As the maximum number of counts per channel increases, χ^2/ν increases even though the

peak shape remains the same. The increase in χ^2/ν does not necessarily mean the fit is inadequate for determining energy calibration or for testing resolution. At low precision, the goodness of fit is dominated by counting statistics; at high precision it is dominated by the inevitable small deviations of the peak shape from a true Gaussian shape, resulting in an increase in the computed value of χ^2/ν. Experience will dictate an acceptable value of χ^2/ν for a given range of peak precision.

Figure 5.6 shows a low-precision spectral peak from a germanium detector (FWHM ~19 channels) with the fitted Gaussian function superimposed upon it. The lower portion of the figure shows the plot of Q(x) versus x for the upper two-thirds of the peak along with the fitted line and the computed peak parameters.

5.1.9 Determination of Peak Position Using a Parabolized Gaussian Fit

The natural logarithm of the Gaussian function is parabolic as is strikingly apparent when full-energy peaks are viewed using the logarithmic display of an MCA. The natural logarithm of the Gaussian (Equation 5-6) gives

$$\ln y = c_2 x^2 + c_1 x + c_0 \qquad\qquad (5\text{-}20)$$

where $c_2 = -1/2\sigma^2$
$\qquad c_1 = x_0/\sigma^2$
$\qquad c_0 = \ln y_0 - x_0^2/2\sigma^2$.

A fit of Equation 5-20 to the set of points $(x_i, \ln y_i)$ produces values of c_2, c_1, and c_0 that give the parameters of the Gaussian:

$$x_0 = -c_1/2c_2$$

$$\sigma = \sqrt{-1/2c_2}$$

$$\ln y_0 = c_0 - c_1^2/4c_2 \ . \qquad\qquad (5\text{-}21)$$

The fitted curve is a parabola that opens downward and whose axis is parallel to the y-axis. The procedure described here determines y_0 in addition to x_0 and σ, the two parameters obtained from the linear fit to the linearized Gaussian. Therefore, the full-energy-peak area can be determined using Equation 5-8.

Figure 5.7 shows a parabolized Gaussian fit to a high-precision spectral peak from the 122.0-keV gamma ray of ^{57}Co. The same high-quality germanium detector was used in this figure as in Figure 5.3(a). At low energies, charge collection in germanium detectors is more complete than at high energies, with a resultant decrease in
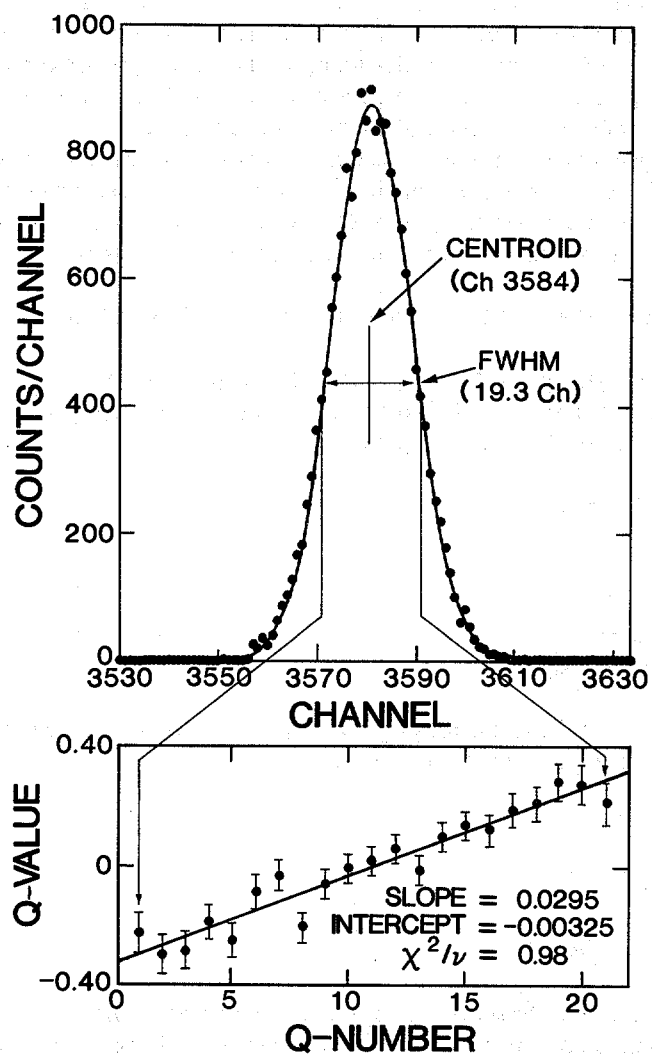
Fig. 5.6 *The upper part of the figure shows a low-precision peak from a high-resolution spectrum to which a linearized Gaussian has been fitted. The lower part shows the plot of $Q(x)$ values and the fitted line.*
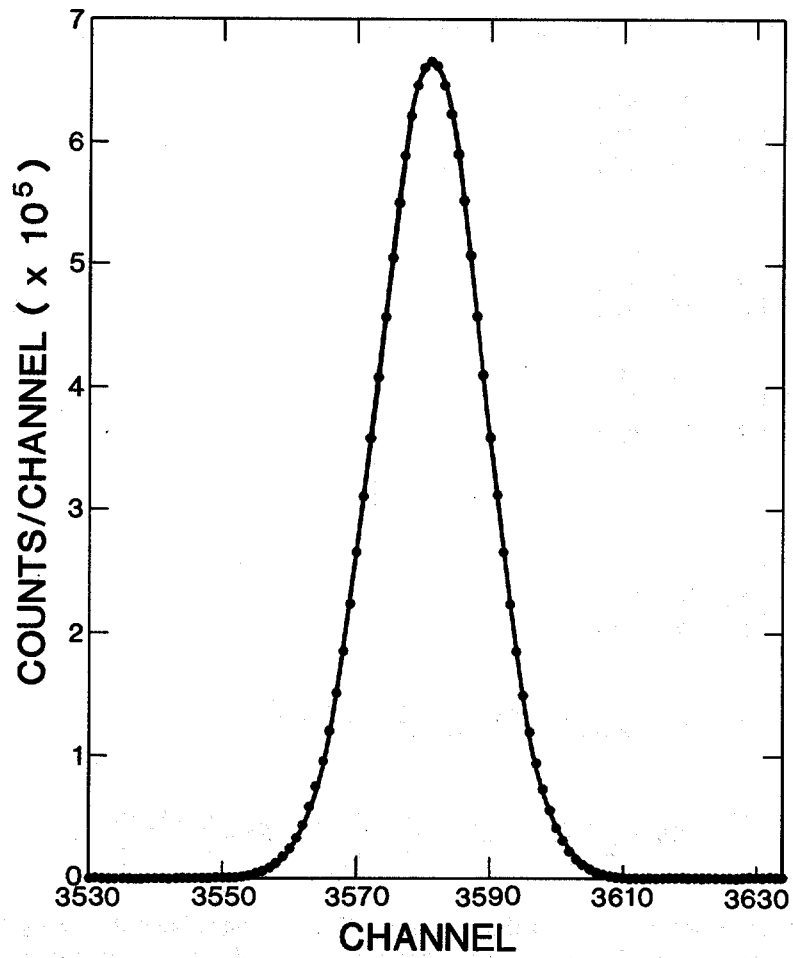
Fig. 5.7 *The 122.0-keV full-energy peak from a ^{57}Co spectrum obtained with a coaxial germanium detector having high resolution and good peak shape. The fitted curve is a "parabolized" Gaussian.*

low-energy tailing. Comparison of Figures 5.3(a) and 5.7 shows that the tailing in the 122-keV peak of Figure 5.7 is even less than the small tailing of the 1332-keV peak in Figure 5.3(a).

The expressions for the weighted quadratic least-squares fit are included for the convenience of possible users. The expressions are given in determinant form and involve eight sums, indicated by S1, S2, ..., S8.

$$
c_0 = \frac{1}{\Delta} \begin{vmatrix} S6 & S2 & S3 \\ S7 & S3 & S4 \\ S8 & S4 & S5 \end{vmatrix}
$$

$$
c_1 = \frac{1}{\Delta} \begin{vmatrix} S1 & S6 & S3 \\ S2 & S7 & S4 \\ S3 & S8 & S5 \end{vmatrix}
$$

(5-22)

$$
c_2 = \frac{1}{\Delta} \begin{vmatrix} S1 & S2 & S6 \\ S2 & S3 & S7 \\ S3 & S4 & S8 \end{vmatrix}
$$

where

$$
\Delta \begin{vmatrix} S1 & S2 & S3 \\ S2 & S3 & S4 \\ S3 & S4 & S5 \end{vmatrix}
$$

$$
S1 = \sum \frac{1}{s_i^2} \quad S2 = \sum \frac{x_i}{s_i^2} \quad S3 = \sum \frac{x_i^2}{s_i^2} \quad S4 = \sum \frac{x_i^3}{s_i^2}
$$

$$
S5 = \sum \frac{x_i^4}{s_i^2} \quad S6 = \sum \frac{\ln y_i}{s_i^2} \quad S7 = \sum \frac{x_i \ln y_i}{s_i^2} \quad S8 = \sum \frac{x_i^2 \ln y_i}{s_i^2} .
$$

As usual, the sums are over all the points fit. The y_i values have the background continuum subtracted. The remaining expressions required for the fitting procedure are

$$
s_i = s(\ln y_i)
$$

$$
s(\ln y) = \frac{s(y)}{\ln y}
$$

(5-23)

where s(y) is given by Equation 5-17. The expression for χ^2/ν, the goodness-of-fit statistic, is

$$\chi^2/\nu = \frac{1}{n-3}\left\{\sum_i \frac{1}{s_i^2}\left[\ln y_i - \left(c_2 x_i^2 + c_1 x_i + c_0\right)\right]^2\right\} \qquad (5\text{-}24)$$

where n is the number of points fit and c_2, c_1, and c_0 are the values computed from Equation 5-22.

The remarks made in the previous section about the portion of the peak to be fit and about trends in χ^2/ν values apply equally well here. The quadratic fits put considerable demands on the computer, and occasionally the six significant decimal digits provided by many 16-bit processors running in single precision are insufficient for performing correct quadratic fits on high-precision data.

5.1.10 Determination of Peak Position Using Complex Spectral Fitting Codes

Large fitting codes are used to analyze complex spectra with overlapping peaks. The codes describe the peaks with functions that have a basic Gaussian form, with tailing functions added to describe the peak shape more accurately. An iterative nonlinear least-squares procedure is used to fit the data. The centroid of the Gaussian component of the fitted peak is taken as the peak position for purposes of energy determination.

5.2 DETECTOR RESOLUTION MEASUREMENTS

5.2.1 Introduction

This section is devoted primarily to the measurement of detector resolution. The importance of good resolution and peak shape in obtaining unbiased NDA results cannot be overemphasized. A narrow, Gaussian peak shape simplifies area determination and minimizes the possibility of bias in assay results.

The full width at half maximum (FWHM or FW.5M) is the basic measure of peak resolution. It is usually given in energy units (keV) for high-resolution detectors and expressed as a percentage of the measurement energy for low-resolution detectors. Resolution measured in energy units increases with energy: $FWHM^2 \approx a + bE$. When expressed as a percentage, resolution decreases with energy.

Most detectors give full-energy peaks that are essentially Gaussian above the half-maximum level. The ratio of the full width at heights less than the half maximum to the FWHM has long been used to quantify the quality of the full-energy-peak shape. Manufacturers measure the FWHM and its ratio to the full width at tenth maximum (FW.1M) to describe the peak shape; for many years a value of FW.1M/FW.5M less than 1.9 was regarded as describing a good peak shape. It is now reasonable to specify FW.02M/FW.5M and even FW.01M/FW.5M when the best peak shape is required.

Table 5-3 gives the theoretical ratios for a Gaussian curve and the measured ratios for a high-quality coaxial germanium detector. The table shows that the actual peak shape closely approaches the Gaussian ideal. The ratios at fiftieth and hundredth maximum should be measured after background subtraction.

Table 5-3. Theoretical and measured resolution ratios

	$\dfrac{FW.1M}{FW.5M}$	$\dfrac{FW.02M}{FW.5M}$	$\dfrac{FW.01M}{FW.5M}$
Gaussian	1.823	2.376	2.578
122.0 keV	1.829	2.388	2.599
	$(1.003)^a$	$(1.005)^a$	$(1.008)^a$
1332.5 keV	1.856	2.428	2.640
	$(1.018)^a$	$(1.022)^a$	$(1.024)^a$

[a] The ratio of the measured ratio to the theoretical ratio for a Gaussian.

The pulse spectrum from a detector is continuous, whereas an MCA or SCA groups the pulses in energy intervals. It is assumed that all the events in an interval can be represented by the energy of the center of the interval. When a Gaussian is fitted to the center points of the intervals, the width parameter σ is slightly greater than that of the original continuous distribution. As discussed in Ref. 8, the grouped variance and the actual variance are related by

$$(\sigma^2)_G = (\sigma^2)_A + h^2/12$$
$$(FWHM^2)_G = (FWHM^2)_A + 0.462h^2 \tag{5-25}$$

where $(\sigma^2)_G$ = grouped variance
$(\sigma^2)_A$ = actual variance
h = group width (MCA channel width or SCA window width).

For MCA spectra, h has units of keV/channel if FWHM is in keV, and $h = 1.00$ if FWHM is in channels. Table 5-4 gives the ratio $(FWHM)_A/(FWHM)_G$. To measure the actual resolution to 0.1%, the system gain should be adjusted to provide more than 15 channels in $(FWHM)_G$. If $(FWHM)_G$ is 3 channels, the $(FWHM)_A$ is overestimated by $\sim 3\%$. The correction has no practical bearing on full-energy-peak areas. The Gaussian function fitted to the binned points has the same area (to better than 0.01%) as the continuous distribution because the y_0 parameter is decreased by almost exactly the same factor as the width parameter is increased.

Table 5-4. The ratio of $(FWHM)_A$ to $(FWHM)_G$

$FWHM_G$ (channels)	$\dfrac{FWHM_A}{FWHM_G}$
3.0	0.9740
5.0	0.9907
10.0	0.9971
15.0	0.9990
20.0	0.9994
25.0	0.9996
30.0	0.9997
35.0	0.9998
40.0	0.9999

5.2.2 Determination of Peak Width by Visual Estimation from MCA Display

Visual estimation works best with MCAs that have horizontal and vertical graticule lines and analog controls for the vertical and horizontal position of the display. Many small MCAs have such features; larger laboratory models usually do not give the user any control over the vertical position of the display.

To determine FWHM to ~1%, the energy gain should be chosen such that FWHM $\geq$ 10 channels. After the spectrum has been accumulated, the display controls are adjusted so that individual channels are resolved and one of the horizontal graticule lines cuts the peak at the half-maximum point. Figure 5.8 shows a peak divided at the half-maximum level. After the peak is bisected, the channels above the horizontal line are counted, estimating to tenths of channels. Because the channels are plotted as points, one really counts the spaces between the points. Usually the continuum on the high-energy side of the peak is regarded as the "bottom" of the peak. The slope of the energy calibration line is used to convert the FWHM value from channels to energy. If the energy calibration is not available, multienergy sources can be used. Large germanium detectors are calibrated with the 122.06- and 136.47-keV gamma rays from ^{57}Co and the 1173.2- and 1332.5-keV gamma rays from ^{60}Co. In either case the energy calibration can be determined from the separation of the peak pair in channels and the known energy difference.* The resolution is then determined by multiplying the FWHM in channels of the 122- or the 1332.5-keV peak and the appropriate energy calibration (keV/channel). With a little practice, values of FWHM (keV) can be determined to within 1%.

---

*Currently the best value for the energy difference between the two ^{57}Co gamma rays is 14.413 keV; the best value for the energy difference between the two ^{60}Co gamma rays is 159.27 keV.
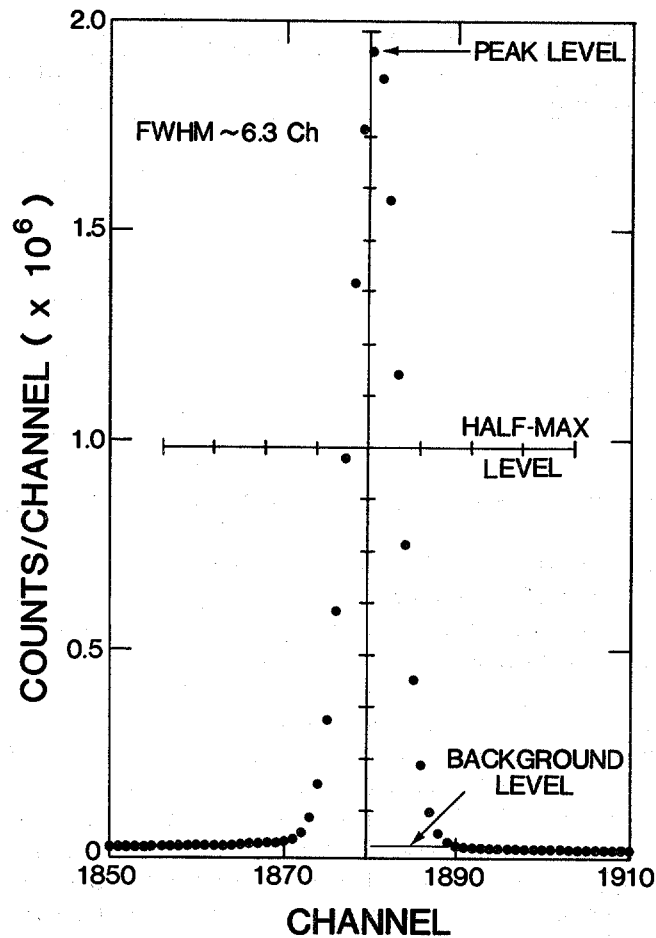
Fig. 5.8 A full-energy peak bisected by the mid-line of an MCA display. The FWHM equals the number of spaces above the half-maximum level.

5.2.3 Graphical Determination of Peak Width

The same type of plot used for energy calibration (Section 5.1.5) may be used for resolution measurement; indeed the two measurements can be combined. The shape of the top of the peak must be sketched to estimate the maximum peak height and the half-maximum line. Figure 5.9 shows the same ^{137}Cs spectrum as shown in Figure 5.4 but indicates the top of the peak, the half-maximum line, and the estimated FWHM.
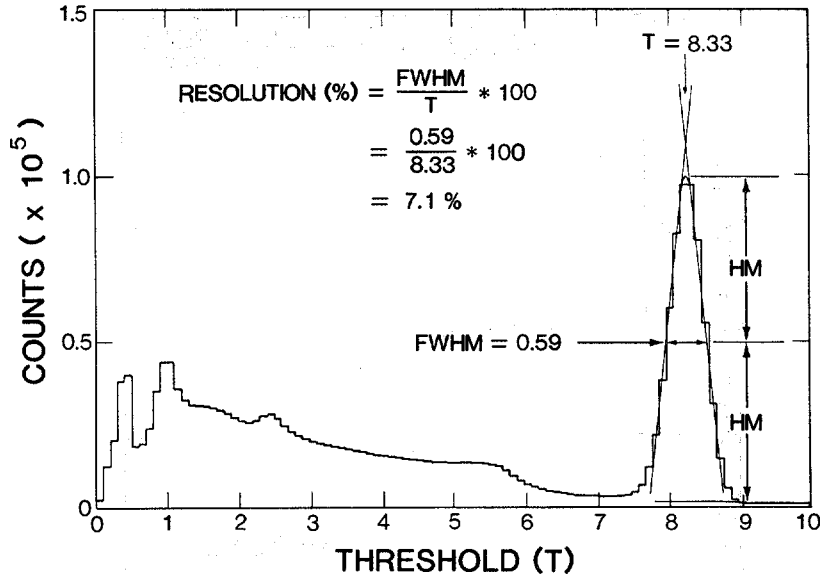
Fig. 5.9 *An SCA-generated spectrum of ^{137}Cs from a NaI(Tl) detector. The plot shows how the FWHM and peak centroid are determined.*

5.2.4 Determination of Peak Width Using Analytical Interpolation

The procedure described here quantifies the graphical procedure presented in the previous paragraph. Most of the FWHM functions built into modern MCA systems use some variation of this procedure. The interpolation procedure is particularly useful because the full width at any fractional height can be determined easily.

Figure 5.10 shows a full-energy peak with the maximum count channel near the centroid. The line across the peak in the figure indicates the fractional height at which the width is evaluated. The x coordinates of the points where the K * maximum line intersects the peak are

$$x_\ell = \frac{Ky_p - y_1}{y_2 - y_1} + x_i$$

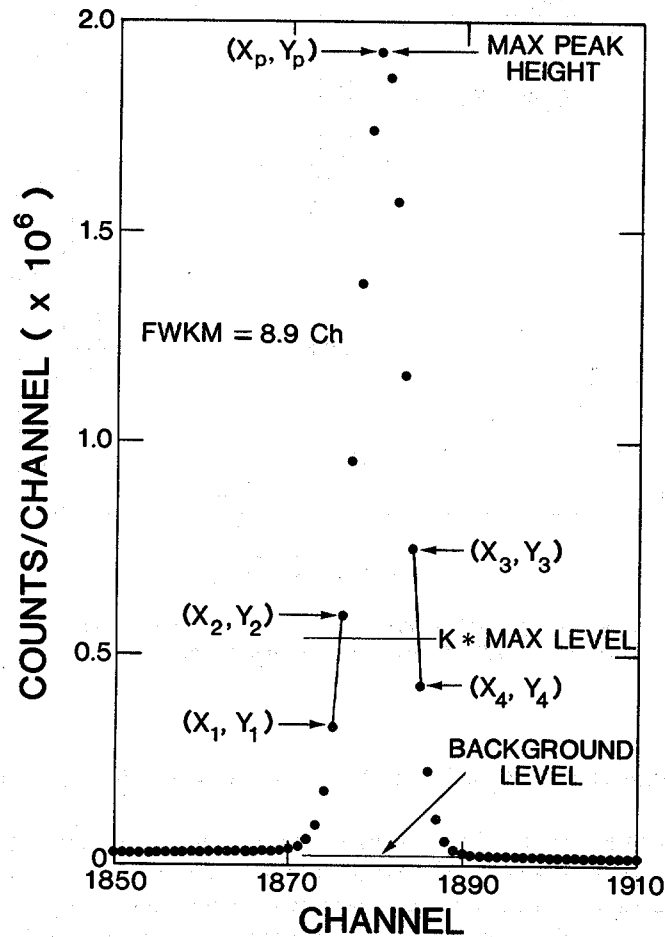$$x_h = \frac{y_3 - Ky_p}{y_3 - y_4} + x_3 \tag{5-26}$$

Fig. 5.10 Diagram of the procedure used to determine the FWKM
by linear interpolation. The value of K may be between
0.0 and 1.0.

where   K = fraction of maximum height at which the width is evaluated
         y_x = number of counts in channel x
         y_p = number of counts in the channel with maximum counts
         x_ℓ = x coordinate of intersection of line K with low-energy side of peak
         x_h = x coordinate of intersection of line K with high-energy side of peak
    x_1, x_2 = channels below and above x_l
    x_3, x_4 = channels below and above x_h.

The full width at the fractional level K (FWKM) is

$$\text{FWKM} = x_h - x_\ell = (x_3 - x_1) + \left[\left(\frac{y_3 - Ky_p}{y_3 - y_4} \right) - \left(\frac{Ky_p - y_1}{y_2 - y_1} \right) \right].$$ (5-27)

To obtain the most accurate results, the value of y_p must be carefully estimated. When two channels with equal counts are at the top of the peak, the maximum value of the peak is clearly higher than the maximum channel value. The maximum channel value underestimates Ky_p and gives a slightly large value for FWKM. The procedure should be applied to peaks that are nearly symmetric about the maximum count channel. The peak maximum y_p can be accurately determined by fitting a Gaussian curve to the upper part of the peak. The peak shape can be accurately determined by using peaks with good statistical precision at all the fractional levels to be measured. For measuring FW.01M, a y_p of $\sim 10^6$ should be used so that the precision at the 0.01 level will still be $\sim 1\%$. Smoothing might be used to obtain consistent results from a peak with poor precision; however, smoothing always broadens the peak a little.

5.2.5 Determination of Peak Width Using the Second-Moment Method

The second-moment method for determining the width parameter σ is analogous to the first-moment method for determining the centroid. The second moment of the normalized Gaussian function is equal to σ^2, the variance of the function. For the unnormalized function in Equation 5-6, the second moment is

$$\sigma^2 = \frac{\int_{-\infty}^{\infty} (x - x_0)^2 \, y(x) \, dx}{\int_{-\infty}^{\infty} y(x) \, dx} \approx \frac{\sum (x_i - x_0)^2 \, y_i}{\sum y_i}.$$ (5-28)

The parameter σ is related to the FWHM by Equation 5-7.

Any significant background continuum should be subtracted before Equation 5-28 is applied. The sums are calculated over a region equal to or larger than three times the FWHM. The method should not be used on peaks with significant asymmetry or with a non-Gaussian shape.

The procedure is useful for broad Gaussian peaks of poor precision where the linear interpolation method does not work well. The first- and second-moment determinations are usually performed together because the centroid value from the first-moment algorithm is required in the second-moment algorithm.

5.2.6 Determination of Peak Width Using a Linearized Gaussian Fit

Section 5.1.8 shows that Equation 5-11 can be used to linearize a Gaussian curve. The slope and intercept of the fitted line are related to the peak centroid and FWHM (Equations 5-7 and 5-13). The linearized Gaussian procedure is a good test of the energy calibration and detector resolution. Testing both a high-energy peak and a low-

energy peak provides strong assurance that the electronic parts of the NDA system are performing correctly. This test can be an important part of a measurement control program for a high-resolution gamma-ray NDA system.

5.2.7 Determination of Peak Width Using a Parabolized Gaussian Fit

Section 5.1.9 shows that the natural logarithm of the Gaussian function is a quadratic function of x. Fitting this function to the set of points $(x_i, \ln y_i)$ gives the parameters of the Gaussian function x_0, y_0, and σ and provides another way of determining the width of a Gaussian peak.

5.3 DETERMINATION OF FULL-ENERGY-PEAK AREA

5.3.1 Introduction

The gamma-ray pulse-height spectrum contains much useful information about gamma-ray energies and intensities. One of the most important concerns in applying gamma-ray spectroscopy is correct extraction of the desired information. Normally, the most important information is the full-energy-peak areas and their associated uncertainties.

Full-energy peaks in gamma-ray pulse-height spectra rest on a background continuum caused by the Compton scattering of higher energy gamma rays. The most fundamental limitation in obtaining unbiased peak areas is the determination of the background continuum. When the continuum is small with respect to the peak, it can cause only a small fractional error in the peak area. However, when the ratio of the peak area to the continuum area becomes much less than 1.0, the possibility of bias rises rapidly.

For many NDA applications, simple background-subtraction methods are adequate. Under certain circumstances, complex spectral fitting codes with long- and short-term tailing functions must be used. With low-resolution detectors, the problem of including small-angle-scattering events in the peak is severe, but computational corrections can sometimes be applied to resolve the problem (Ref. 9).

5.3.2 Selection of Regions of Interest (ROIs)

The choice of ROI is as important as the choice of algorithms used to evaluate peak areas. Most procedures use two ROIs to define the continuum level on the low- and high-energy sides of a peak or multiplet. The average channel count of an ROI is taken as the continuum level at the center of the ROI. A third ROI defines the peak region.

For a Gaussian function, 99.96% of the area lies within a region centered at x_0 that is three times the FWHM of the function. The amplitude of the Gaussian function at

$x_0 \pm 1.75$ FWHM is only 0.0082% of the maximum value at x_0 so continuum ROIs that begin at this point have minimal contributions from the peak. Thus, a peak ROI of three times the FWHM and continuum ROIs placed symmetrically 3.5 to 4.0 times the FWHM apart should obtain ~99.9% of the peak area.

In principle, the continuum is estimated more precisely if the continuum ROIs are quite wide. However, the possibility of systematic error increases as the energy interval increases. For most NDA applications, continuum ROIs of 0.5 to 1.0 times the FWHM are adequate. With an energy calibration of 0.1 keV/channel, typical background ROIs are three to five channels wide. When the continuum between neighboring peaks is very narrow, ROIs of one or two channels must be used. Peaks whose centers are separated by three times the FWHM can be considered resolved; usually a narrow ROI can be placed between them. It is better to sacrifice statistical precision than to introduce bias by using continuum ROIs that are too wide.

Spectra with significant low- or high-energy tailing may require a wider peak ROI than three times the FWHM. Because peak resolution deteriorates somewhat at high rates, the ROI should be set on a high-rate (low-resolution) spectrum. Usually, better results are obtained if all the ROIs are of equal width; therefore, the ROIs for low-energy peaks and reference pulser peaks are somewhat wider than three times the FWHM.

Computer codes can be written to accurately and consistently choose ROIs. Digital stabilization can be used to keep the desired peaks within a single preselected set of ROIs for long time periods. Sometimes it is desirable to change the spectrum to fit a particular set of ROIs. Codes exist that can reshuffle the contents of a spectrum to give any desired energy calibration with little degradation of spectral quality.

5.3.3 Subtraction of Straight-Line Compton Continuum

It is often adequate to approximate the Compton continuum by a straight line between the high- and low-energy sides of well-resolved peaks or of overlapping peak groups. Figure 5.11 shows how the ROIs are selected and indicates the notation used in the background equations. Note that the continuum ROIs need not be symmetrically placed with respect to the peak ROI nor need they be of equal width. The background is the trapezoidal area beneath the continuum line given by

$$B = [Y(F_p) + Y(L_p)] (N_p/2) \tag{5-29}$$

where $Y(F_p) = mF_p + b$

$\qquad Y(L_p) = mL_p + b$

and where $m = (Y_h - Y_\ell)/(X_h - X_\ell)$

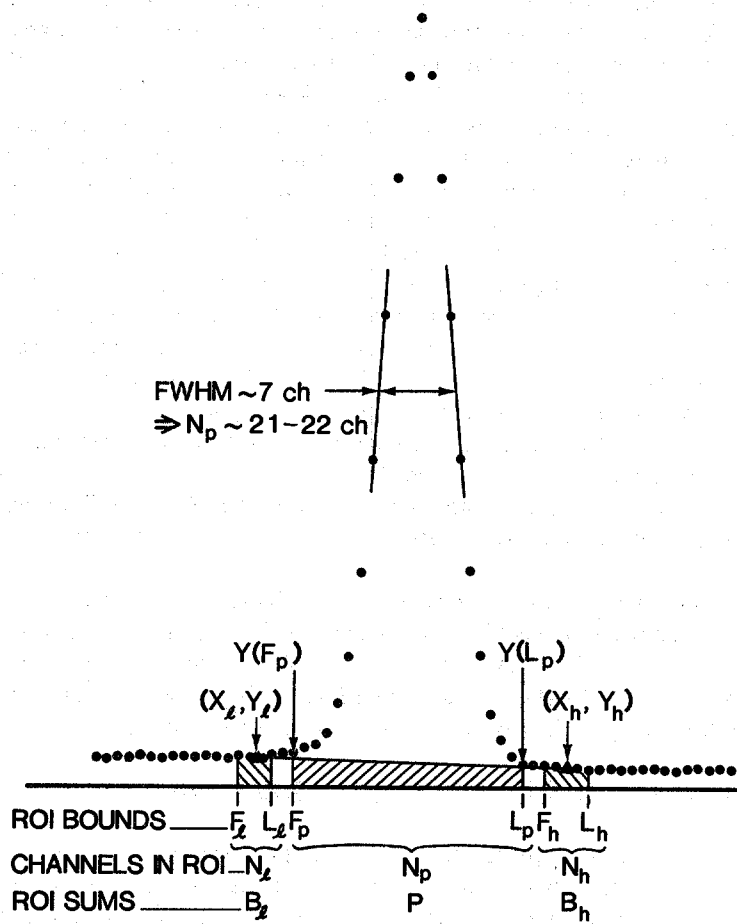$\qquad b = (X_h Y_\ell - X_\ell Y_h)/(X_h - X_\ell)$.

Fig. 5.11 Regions of interest and associated parameters used to compute the net area and the estimated standard deviation of a full-energy peak.

The variance of the background B is

$$S^2(B) = \left(\frac{N_p}{2}\right)^2 \left[K^2 \frac{B_h}{N_h^2} + (2 - K)^2 \frac{B_\ell}{N_\ell^2}\right]$$ (5-30)

where $K = \dfrac{(F_p + L_p - 2X_\ell)}{(X_h - X_\ell)}$.

Equation 5-30 assumes no uncertainty in the ROI bounds and is a function only of the statistical uncertainties in B_h and B_ℓ, which are estimated by $S^2(B_\ell) = B_\ell$ and $S^2(B_h) = B_h$. Equation 5-30 is correct when the background ROIs are not symmetrically placed relative to the peak ROI. If the continuum ROIs are placed symmetrically relative to the peak ROI, the expressions for both B and $S^2(B)$ are simplified. The symmetry requirement means that $(F_p - X_\ell) = (X_h - L_p)$ and $K = 1$, and so the expressions become

$$B = \left(\frac{Y_\ell + Y_h}{2}\right)N_p = \left(\frac{B_h}{N_h} + \frac{B_\ell}{N_\ell}\right)\frac{N_p}{2} \tag{5-31}$$

and

$$S^2(B) = \left(\frac{N_p}{2}\right)^2 \left(\frac{B_h}{N_h^2} + \frac{B_\ell}{N_\ell^2}\right). \tag{5-32}$$

Frequently Equations 5.31 and 5.32 are used even when the symmetry requirement is not met, and if the net peak areas are much greater than the subtracted continuum, little error will result. However, when the peak areas are equal to or less than the subtracted continuum, the error may well be significant. In dealing with complex spectra (the spectra of plutonium are good examples), one is frequently forced to use asymmetrically placed ROIs. When the required computations are performed by interfaced processors, Equations 5-29 and 5-30 should be used because they give the best results that can be obtained with any version of the straight-line procedure.

For computations done with a small calculator, the use of the simplest possible expression is desirable and ROIs should be chosen accordingly. If $N_h = N_\ell \equiv N_c$, Equations 5-31 and 5-32 simplify to

$$B = \frac{N_p}{2N_c}(B_h + B_\ell) \tag{5-33}$$

and

$$S^2(B) = \left(\frac{N_p}{2N_c}\right)^2 (B_h + B_\ell). \tag{5-34}$$

If it is possible to choose $N_c = N_p/2$, the expressions achieve the simplest forms:

$$B = (B_h + B_\ell) \tag{5-35}$$

and

$$S^2(B) = (B_h + B_\ell) = B . \tag{5-36}$$

5.3.4 Subtraction of Smoothed-Step Compton Continuum

The Compton continuum beneath a full-energy peak is not a straight line. At a given energy, most of the continuum is caused by large-angle Compton scattering of higher energy gamma rays or by pulse pileup from lower energy interactions. The part of the continuum under a peak that is caused by the gamma ray that generates the peak results from small-angle Compton scattering and full-energy events with incomplete charge collection; this contribution can be described by a smoothed step function.

Gunnink (Ref. 10) devised the original procedure to generate a step-function continuum beneath single peaks or multiplets based on the overlying spectral shape. The procedure provides better results than the straight-line background approximation, especially for overlapping peak multiplets. For clean single peaks, the improvement is often negligible.

Figure 5.12 shows a logarithmic plot of a multiplet and a step-function background. Using the notation of Figure 5.11, the background at channel n is

$$B_n = Y_\ell - D\left[\sum_{i=X_\ell+1}^{i=n} (y_i - Y_h) \bigg/ \sum_{i=X_\ell+1}^{i=X_h} (y_i - Y_h)\right] \qquad (5\text{-}37)$$

where y_i = total counts in channel i

$D = Y_\ell - Y_h$

$B(X_\ell) = Y_\ell$

$B(X_h) = Y_h.$

The background Y_h is subtracted from every channel because the Compton events from higher energy gamma rays cannot influence the shape of the smoothed step for lower energy gamma rays. Equation 5-37 is usable when the continuum beneath a peak or multiplet has a slightly negative or zero slope.

A significant complication in using the smoothed-step procedure is that the expression for the precision of the net area becomes exceedingly complicated when derived from Equation 5-37. The precision expression (Equation 5-30) based on the straight-line approximation is much simpler and almost as accurate.

5.3.5 Subtraction of Compton Continuum Using a Single Region of Interest

Estimating the background continuum from a single ROI is sometimes desirable or necessary. For example, a single ROI is often desirable when using a NaI detector and a single-channel analyzer (SCA) to measure ^{235}U enrichment or ^{239}Pu holdup.
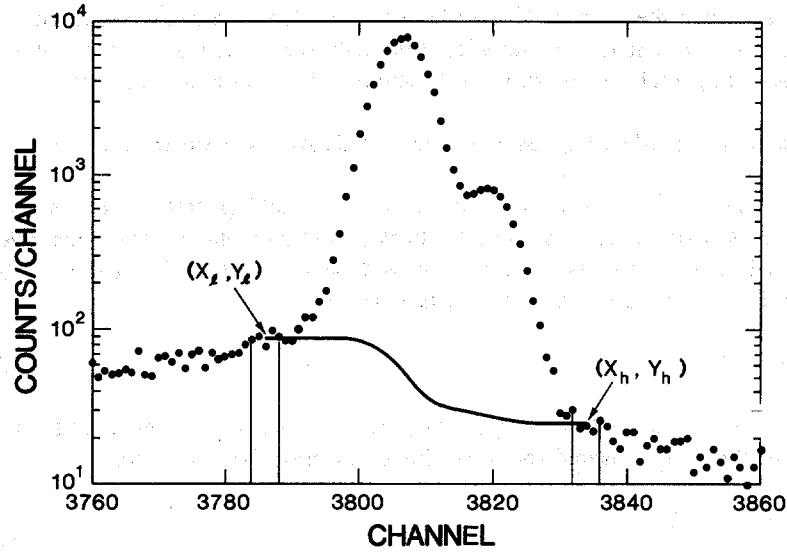
Fig. 5.12 *A peak doublet with the estimated spectral continuum computed by the simple smoothed-step algorithm.*

When the signal-to-background ratio is high, it may be adequate to assume a flat background continuum. Here, the contribution of the continuum to the peak ROI is given by

$$B = \frac{N_p}{N_h} B_h \tag{5-38}$$

$$s(B) \approx \frac{N_p}{N_h} s(B_h) \ . \tag{5-39}$$

Although this procedure is most often used with low-resolution scintillators, it is also used with germanium detectors when there is no convenient place for a background ROI on the low-energy side of a peak.

If the background continuum is not flat but can be assumed to have a constant slope over the energy range concerned, Equation 5-38 may be modified to

$$B = KB_h \tag{5-40}$$

where K is a constant factor determined by experiment. If the ambient background radiation is the main contributor to the Compton continuum, a "no sample" spectrum may be used to determine K. If the continuum is strongly dominated by high-energy

gamma rays from the sample, K may be estimated from an MCA spectrum. Often K will change from sample to sample. Although these single-ROI procedures have limited accuracy, their use is preferred to ignoring the continuum problem entirely.

5.3.6 Subtraction of Compton Continuum Using Two-Standard Procedures

Measurement of ^{235}U enrichment using the 185.7-keV gamma ray is a successful application of a single SCA window for background corrections. The assumption of a constant background shape is very good, and the constant K of Equation 5-40 can be determined accurately. The enrichment E is given by

$$E = C(P - KB) \tag{5-41}$$

where C is a constant with units (% ^{235}U/count). For two samples of different and known enrichments measured for equal times, Equation 5-41 becomes

$$E_1 = C(P_1 - KB_1) \tag{5-42}$$

$$E_2 = C(P_2 - KB_2) .$$

The solution to these equations is

$$C = (E_2B_1 - E_1B_2)/(P_2B_1 - P_1B_2) .$$

$$K = (E_2P_1 - E_1P_2)/(E_2B_1 - E_1B_2) . \tag{5-43}$$

Equation 5-41 may be written as

$$E = aP - bB \tag{5-44}$$

where

$$a = \frac{E_2B_1 - E_1B_2}{P_2B_1 - P_1B_2}$$

$$b = \frac{P_1E_2 - P_2E_1}{P_2B_1 - P_1B_2} . \tag{5-45}$$

The two-standard method can be used to measure low-level radioactive contaminations in water or other fluids. See Chapter 7 on uranium enrichment for more details on this procedure.

5.3.7 Using Region-of-Interest Sums to Measure Peak Areas

For well-resolved peaks, the simple summation of counts above the estimated background continuum is probably as good as any other method of finding the peak area. This method avoids any difficulty from imperfections in the peak-shape models of spectral fitting codes. The ROI-summation method is quite tolerant of small variations in peak shape and provides an accurate and straightforward estimate of the precision of the net peak area.

For all ROI-summation procedures, the peak area is given by

$$A = P - B \tag{5-46}$$

where P is the integral of the peak ROI and B is the contribution from the background continuum. The expressions for $S^2(A)$, the estimated variance of the net area, vary according to the procedure used to estimate the background continuum.

When B is estimated by straight-line interpolation from continuum ROIs on either side of the peak ROI, the estimated variance of the peak area is

$$S^2(A) = S^2(P) + S^2(B) = P + S^2(B) . \tag{5-47}$$

Equations 5.29 through 5.36 give B and $S^2(B)$ for different conditions on the width and position of the background ROIs relative to the peak ROI. The expressions are summarized in Table 5-5. The simplest expressions are obtained when the background ROIs are symmetrically placed with respect to the peak ROI and have the appropriate widths. When adequate computational capacity is available, the most general form of the expressions should be used so that ROIs can be assigned without constraint.

When the smoothed step function is used to estimate the background continuum, Equations 5-46 and 5-37 combine to give

$$A = P - \sum_{n=F_p}^{L_p} \left\{ Y_\ell - D \left[\sum_{i=X_\ell+1}^{n} (y_i - Y_h) \bigg/ \sum_{i=X_\ell+1}^{X_h} (y_i - Y_h) \right] \right\} . \tag{5-48}$$

Because the continuum estimate is a function of the channel counts, the exact expressions for $S^2(A)$ become extremely complex. One of the estimates for $S^2(A)$ given in Table 5-5 should be used.

Table 5-5. Expressions for net full-energy-peak areas and estimated variances[a] (straight-line background assumed)[b]

Conditions on ROIs	Background B	Background Variance $S^2(B)$
Arbitrary position and width of background ROIs	$B = [Y(L_p) + Y(F_p)](N_p/2)$ where $Y(L_p) = mL_p + b$ and $Y(F_p) = mF_p + b$ and where $m = (Y_h - Y_\ell)/(X_h - X_\ell)$ and $B = (X_h Y_\ell - X_\ell Y_h)/(X_h - X_\ell)$	$S^2(B) = \dfrac{N_p^2}{2}\left[K^2\dfrac{B_h}{N_h^2} + (2-K)^2\dfrac{B_\ell}{N_\ell^2}\right]$ where $K = \dfrac{2(X - X_\ell)}{(X_h - X_\ell)} = \dfrac{(F_p + L_p - 2X_\ell)}{(X_h - X_\ell)}$.
Symmetric placement of background ROIs relative to peak ROI, $(F_p - X_\ell) = (X_h - L_p)$	$B = \dfrac{N_p}{2}(Y_h + Y_\ell) = \dfrac{N_p}{2}\left(\dfrac{B_h}{N_h} + \dfrac{B_\ell}{N_\ell}\right)$	$S^2(B) = \left(\dfrac{N_p}{2}\right)^2\left(\dfrac{B_h}{N_h^2} + \dfrac{B_\ell}{N_\ell^2}\right)$

Table 5-5. (CONT.)

Symmetric placement of background ROIs with $N_\ell = N_h = N_c$	$B = \dfrac{N_p}{2N_c}(B_h + B_\ell)$	$S^2(B) = \left(\dfrac{N_p}{2N_c}\right)^2 (B_h + B_\ell)$
Symmetric placement of background ROIs with $N_\ell = N_h = N_p/2$	$B = (B_h + B_\ell)$	$S^2(B) = (B_h + B_\ell) = B$

$^a A = P - B$

  $S^2(A) = P + S^2(B)$.

^{b}Notation summary as in Figure 5.11; LE = low energy; HE = high energy:

F_ℓ, L_ℓ	= first and last channels of LE background ROI
F_p, L_p	= first and last channels of peak ROI
F_h, L_h	= first and last channels of HE background ROI
B_ℓ, P, B_h	= integrals of LE background, peak, and HE background ROIs
N_ℓ, N_p, N_h	= numbers of channels in LE background, peak, and HE background ROIs
$Y_h = B_h/N_h$	= average continuum level in HE background ROI
$Y_\ell = B_\ell/N_\ell$	= average continuum level in LE background ROI
X_h, x_ℓ	= centers of background ROIs
$Y(F_p)$ and $Y(L_p)$	= ordinates of background line at F_p and L_p
m and b	= slope and intercept of background line between (X_ℓ, Y_ℓ) and (X_h, Y_h).

When a single background ROI is used, Equation 5-46 holds for the net peak area, and the expression for $S^2(A)$ is based on Equation 5-47. When the continuum is assumed to be flat (Equation 5-38), the expressions for A and $S^2(A)$ become

$$A = P - \frac{N_p}{N_h} B_h$$

$$S^2(A) = P + \left(\frac{N_p}{N_h}\right)^2 B_h \ . \tag{5-49}$$

If a sloped continuum is assumed (Equation 5-40), the expressions for A and $S^2(A)$ become

$$A = P - KB_h$$
$$S^2(A) = P + K^2 B_h \ . \tag{5-50}$$

Note that although Equations 5-49 and 5-50 may correctly predict the repeatability of measurements, they do not predict any assay bias arising from the approximate nature of the single-ROI background estimate.

5.3.8 Using Simple Gaussian Fits to Measure Peak Areas

As shown in Section 5.1.3, the determination of σ and y_0 by a Gaussian fit also determines the peak area using Equation 5-8. For cleanly resolved peaks, the areas obtained by fitting simple Gaussians are probably no better than those obtained from ROI sums, and may be somewhat worse. This assertion is known to be true for germanium detectors. For NaI scintillators, a Gaussian fit may give more consistent peak areas than ROI methods. The simple Gaussian-fitting procedures do not provide straightforward ways to estimate peak-area precision.

In a few situations, Gaussian fitting is advantageous. When two peaks are not quite resolved such that the desired peak ROIs overlap, a Gaussian can be fitted to one-FWHM-wide ROIs centered on each peak to determine the peak areas. When the centroid location and FWHM are the primary information desired from a Gaussian fit, the area estimate often comes with no extra effort. When a peak has significant low-energy tailing from Compton scattering in the sample or shielding, a simple Gaussian fit to the middle FWHM of the peak can easily obtain the desired area.

When a Gaussian function is transformed to a line that is least-squares fit to obtain the parameters x_0 and σ, the parameter y_0 can also be determined using any of the original data points and Equation 5-6 to solve for y_0. An average of the values of y_0 determined from several points near x_0 gives a satisfactory value for the area equation.

Section 5.1.9 shows that the logarithm of the Gaussian function is parabolic and that a quadratic fit to $\ln(y_i)$ yields all three of the Gaussian parameters x_0, y_0, and σ. The peak area is obtained from Equation 5-8. As with the linearized Gaussian procedure, no simple expressions exist to estimate the precision of the peak areas.

5.3.9 Using Known Shape Parameters to Measure Peak Areas in Multiplets

The previous discussion emphasizes well-resolved single peaks because most applications of gamma-ray spectroscopy to the NDA of nuclear material employ well-resolved peaks. However, to measure isotopic ratios from high-resolution plutonium spectra, it is necessary to analyze unresolved peak multiplets.

If the peak shape is described by an adequate mathematical model in which all the parameters are known except the amplitude, unresolved multiplets can be analyzed quite simply by ordinary noniterative least-squares methods. For some purposes the simple Gaussian function (Equation 5-6) is adequate without any tailing terms. If the position and width parameters x_0 and σ are known, only the amplitude parameter y_0 is unknown. Frequently, the well-resolved peaks in a spectrum can yield sufficient information to determine the x_0 and σ parameters for the unresolved peaks. The gamma-ray energies are accurately known for all fissionable isotopes; therefore, the energy calibration can be determined with sufficient accuracy to calculate the x_0 parameter for all unresolved peaks. The width parameter σ can be determined from the well-resolved peaks and interpolated to the unresolved peaks with the relation $FWHM^2 = a + bE$, which is quite accurate for germanium detectors above 100 keV. The well-resolved peaks can also yield information needed to determine the parameters of tailing terms in the peak-shape function.

The least-squares fitting procedure for determining the peak amplitudes is most easily described by the following example. The example assumes a three-peak multiplet where all the peaks come from different isotopes. After the Compton continuum is subtracted from beneath the multiplet, the residual spectrum has only the three overlapping peaks and the count in channel i may be written as

$$y_i = A1 \times F1_i + A2 \times F2_i + A3 \times F3_i \tag{5-51}$$

where A1, A2, and A3 are the amplitudes to be determined and F1, F2, and F3 are the functions describing the peak shapes. Assuming that the peaks are well described by a pure Gaussian,

$$F1 = \exp[K1(x_i - x1_0)^2]$$
$$F2 = \exp[K2(x_i - x2_0)^2]$$
$$F3 = \exp[K3(x_i - x3_0)^2] \tag{5-52}$$

where $x1_0$, $x2_0$, $x3_0$ = known centroid positions

$\quad$ K1, K2, K3 = $1/2\sigma^2_{1,2,3}$

$$\sigma_i = (FWHM)_i / \left(2\sqrt{2\ln 2}\right) .$$

The least-squares fitting procedure determines A1, A2, and A3 to minimize the sum of the squared difference between the actual data points and the chosen function. With derivation the expressions for A1, A2, and A3 are

$$A1 = \frac{1}{D}\begin{vmatrix} \sum yF1 & \sum F1\,F2 & \sum F1\,F3 \\ \sum yF2 & \sum F2^2 & \sum F2\,F3 \\ \sum yF3 & \sum F3\,F2 & \sum F3^2 \end{vmatrix}$$

$$A2 = \frac{1}{D}\begin{vmatrix} \sum F1^2 & \sum yF1 & \sum F1\,F3 \\ \sum F2\,F1 & \sum yF2 & \sum F2\,F3 \\ \sum F3\,F1 & \sum yF3 & \sum F3^2 \end{vmatrix}$$

$$A3 = \frac{1}{D}\begin{vmatrix} \sum F1^2 & \sum F1\,F2 & \sum yF1 \\ \sum F2\,F3 & \sum F2^2 & \sum yF2 \\ \sum F3\,F1 & \sum F3\,F2 & \sum yF3 \end{vmatrix}$$

$$D = \begin{vmatrix} \sum F1^2 & \sum F1\,F2 & \sum F1\,F3 \\ \sum F2\,F1 & \sum F2^2 & \sum F2\,F3 \\ \sum F3\,F1 & \sum F3\,F2 & \sum F3^2 \end{vmatrix} \tag{5-53}$$

The pattern of Equation 5-53 can be followed for expanding to additional unknowns. The form of F1, F2, and F3 is not related to the solutions for A1, A2, and A3. The only requirement is that the functions are totally determined except for an amplitude factor. Tailing terms may be added to improve the accuracy of the peak-shape description. When two or more peaks in a multiplet are from the same isotope, the known branching intensities, I_1, I_2 ..., can be used to fit the peaks as a single component. If peaks one and two in the example are from the same isotope, Equation 5-51 becomes

$$y_i = A \times F_i + A3 \times F3_i \tag{5-54}$$

where

$$F = \exp[K1(x_i - x1_0)^2] + (I_2/I_1)\exp[K2(x_i - x2_0)^2].$$

Equation 5-54 has only two unknowns, A and A3. Strictly speaking, the coefficients in F should be $1/E_1$ and $I2/I_1E_2$ where E1 and E2 are the relative efficiencies at the two energies. If available, the efficiencies should be included, but often the related members of the multiplet are so close together in energy that $E1 \approx E2$. When one of the related gamma rays is much more intense than the other, the errors in the intense components caused by assuming E1 = E2 are usually negligible.

5.3.10 Using Complex Fitting Codes to Measure Peak Area

Much time has been invested in the development of computer codes to determine the peak areas from complex, overlapping peak multiplets. A number of successful codes exist, along with many variations for special problems. Helmer and Lee (Ref. 11) review the peak models and background subtraction procedures of most currently used codes.

The complex codes describe full-energy peaks with a basic Gaussian shape plus one or two low-energy tailing terms (long- and short-term tailing) and sometimes a high-energy tailing term. The long-term tail is often not included in the full-energy-peak area because it is ascribed to small-angle Compton scattering within the sample. The long-term tailing function usually is not required for high-resolution spectra. The detailed form of the tailing terms varies from code to code, although the results are often equivalent. The procedures to subtract the Compton continuum also vary; in general, the background subtraction procedures are most in need of improvement.

These fitting codes are often indispensable, but they often require a major learning effort before they can be used intelligently. Learning to use such codes skillfully can be likened to learning to play a large pipe organ; after acquiring some basic skills, one must learn the possibilities and limitations of the many combinations of "stops." The potential user who does not have extensive experience in gamma-ray spectroscopy should consult with knowledgeable users of the code.

Note that all fitting codes perform better on high-quality spectra with good resolution and minimal peak tailing. A fitting code cannot completely compensate for poor-quality detectors and electronics or for sloppy acquisition procedures. It should be said that an ounce of resolution is worth a pound of code. In the past few years, the quality of detectors and electronics has improved in parallel with code development, resulting in the present ability to do measurements that were previously very difficult, if not impossible.

5.4 RATE-RELATED LOSSES AND CORRECTIONS

5.4.1 Introduction

As discussed in Chapter 4, ADC deadtime is defined as the sum of the time intervals during which the ADC is unable to process other events. Deadtime can occur in all NDA system components. The deadtime intervals are either fixed or are a function of system parameters and pulse amplitude.

For MCA-based systems, the deadtime begins when the amplifier output pulse crosses the ADC discriminator threshold. The deadtime includes the pulse risetime, a small fixed time for peak detection and latching, a digitization time, and often the memory storage time. For germanium detector systems using 100-MHz Wilkinson ADCs, the deadtime for an event at channel 4000 is ~55 μs. At rates of only a few thousand counts per second, a significant fraction of information can be lost to system deadtime alone.

For SCA-based systems using NaI(Tl) detectors, the deadtime is much shorter and can often be ignored. The losses in such systems are usually due to pulse pileup.

Pulse pileup is described briefly in Chapter 4. Figure 4.9 shows how two events that occur within an interval less than the amplifier pulse width sum to give a pulse whose amplitude is not proportional to either of the original pulses. Figure 4.10 shows the effect of pileup events on the spectrum. Pileup can occur in the detector, the preamplifier, or the main amplifier, but the overall effect is governed by the slowest component, usually the main amplifier. Pileup always results in a loss of information; the degree of loss depends on the information sought and the gross count rates involved. For example, when counting events above a discriminator threshold, two pileup events are counted as one; if pulse-height analysis is being performed, both events are lost from their respective peaks.

In high-resolution spectroscopy systems, the amplifier pulse width is often comparable to the ADC processing time, and the loss of information caused by pileup may be equal to or greater than the loss caused by deadtime. Although an MCA can operate in a live-time mode and compensate for deadtime losses, it does not fully compensate for pileup losses.

Many texts discuss all counting losses in terms of two limiting cases, both of which are referred to as deadtime [see, for example, Chapter 3 of Knoll (Ref. 12)]. Neither case exactly describes the operation of actual equipment. One case is called nonparalyzable deadtime and is typical of ADC operation; the other is termed paralyzable deadtime and is related to pulse pileup. The terminology is unfortunate because no circuitry is dead during pileup; rather, events are lost from their proper channel because of the pulse distortion. In this book the distinction between deadtime and pileup is preserved because they are two distinctly different loss mechanisms.

The goal of many gamma-ray spectroscopy applications is to compute a corrected rate CR for the gamma ray(s) of interest:

$$CR = RR \times CF(RL) \times CF(AT) \tag{5-55}$$

where RR = raw rate of data acquisition
  CF(RL) = rate-related loss correction factor
  CF(AT) = attenuation correction factor (See Chapter 6).

When the correction factors are properly defined and computed, CR is the count rate that would be observed if there were no electronic losses and no sample attenuation. The corrected rate CR is often directly proportional to the desired quantity, such as mass of ^{239}Pu or ^{235}U enrichment. All three factors in Equation 5-55 must be determined accurately to obtain accurate assays.

5.4.2 Counting Loss as a Function of Input Rate

In modern spectroscopy systems, counting losses are rarely well described by the simple model of nonparalyzable deadtime; however the model is described here for completeness. In early systems, the deadtime losses were far higher than pileup losses, and the simple nonparalyzable model was quite adequate.

For a fixed deadtime D, CR can be represented as follows:

$$CR = \frac{RR}{1 - RR \times D} . \tag{5-56}$$

Inverting Equation 5-56 gives

$$RR = \frac{CR}{1 + CR \times D} = \frac{1}{1/CR + D} . \tag{5-57}$$

As CR → ∞, RR → 1/D as a limiting value of throughput. The term nonparalyzable arises because RR rises monotonically toward the limit 1/D. For pileup losses, RR → 0 as CR → ∞, justifying the term paralyzable.

Although Wilkinson ADCs do not have a fixed deadtime, Equations 5-56 and 5-57 apply if D is set equal to the average deadtime interval. Whether fixed or an average, the deadtime D is rarely determined directly because most users wish to correct for the combined rate-related losses.

Pulse-pileup losses are important in high-resolution spectroscopy for two reasons. First, the relatively long pulse-shaping times required for optimum signal-to-noise ratio yield pulse widths up to 50 μs, which increases the probability of pileup. Second, a small pileup distortion can throw a pulse out of a narrow peak. Because NaI(Tl)

systems operate with time constants of $\sim$3 μs or less, they have lower pileup losses. Furthermore, because the NaI peaks are 10 to 20 times broader than germanium peaks, many events can suffer a slight pileup and still remain within the full-energy peak. However, pileup losses in NaI(Tl) spectra are much harder to correct because of the broader peaks.

Figure 5.13 shows that if an amplifier pulse is preceded or followed by a pulse within approximately half the pulse width, its peak amplitude is distorted. The degree of distortion depends on the amplitude and timing of the interfering pulse relative to the analyzed pulse. Frequently pileup-rejection circuitry is used to detect and prevent analysis of the distorted events. Unfortunately, in rejecting bad pulses almost all systems reject some small fraction of nondistorted pulses.

If no other events occur within the time interval T where pileup is possible, the pulse will be analyzed and stored in its proper location. The fundamental expression from Poisson statistics (Refs. 1 and 3) that applies here is

$$P(N) = \frac{(RT)^N e^{-RT}}{N!} \tag{5-58}$$

where P(N) is the probability of N events occurring within a time interval T if the average rate is R. The probability that an event is not lost to pileup is obtained by setting N = 0 in Equation 5-58:

$$P(0) = e^{-RT} . \tag{5-59}$$

The fraction F of pulses lost to pileup is given by

$$F = 1 - P(0) = 1 - e^{-RT} . \tag{5-60}$$

If RT is much less than 1, Equation 5-60 simplifies to

$$F \approx RT \tag{5-61}$$

which provides a very simple relationship for estimating the pileup losses at lower rates.

If deadtime losses can be ignored, Equation 5-59 describes the throughput of a high-resolution spectroscopy system. The measured raw rate RR is given by

$$RR = Re^{-RT} \tag{5-62}$$

where R is the gross rate of events from the detector. Differentiation of Equation 5-62 shows that RR is maximized at R = 1/T and that the fraction of R stored at that rate is 1/e $\approx$ 0.37. Thus, at the input rate for maximum throughput, just over a third of the input events are correctly analyzed and stored. The fraction of the input rate that is stored is e^{-RT}, and the stored rate as a fraction of the maximum stored rate 1/(eT) is given by RTe^{1-RT}. Both of these fractions are plotted in Figure 5.14.
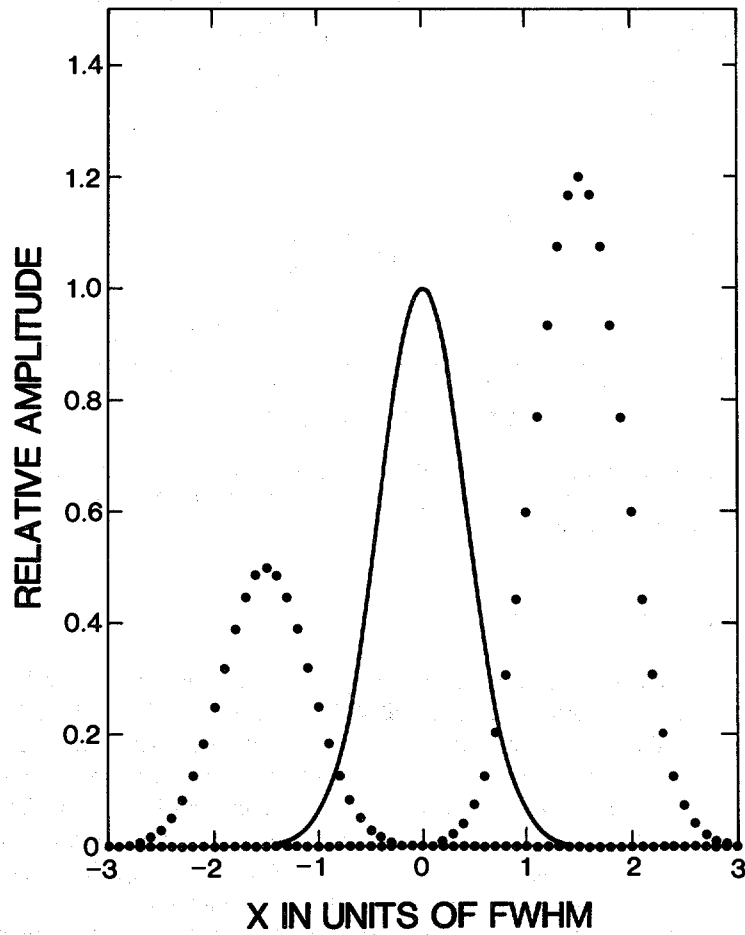
Fig. 5.13 *Three Gaussian curves (amplifier pulses) separated by 1.5 × FWHM. As drawn, there is minimal pileup distortion to any pulse. If the pulse separation is reduced, the distortion will clearly increase.*
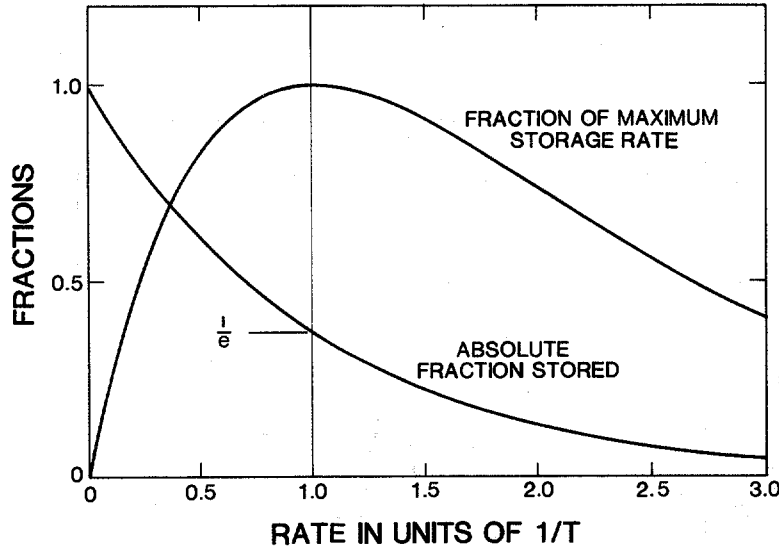
Fig. 5.14 *The absolute fraction stored and the fraction of the maximum storage rate for a paralyzable system of deadtime T as a function of input rate in units of 1/T.*

5.4.3 Actual Data Throughput

Figure 5.14 shows that the throughput rate peaks at surprisingly low values for ordinary high-resolution gamma-ray spectroscopy systems. For $T = 50$ μs (a high though common value), $1/T = 20\ 000$ s^{-1} and the maximum throughput is about 7350 s^{-1}. Where long time constants are necessary to produce the desired resolution, throughput must be sacrificed as the price for the highest resolution. In fact, the low-rate side of the throughput curve should be used when possible because it yields better resolution and peak shape. At a rate of $0.6(1/T)$, the throughput is 90% of maximum; at only $0.5(1/T)$, the throughput is still 82% of maximum.

Sometimes a spectroscopy system must be operated far beyond the throughput maximum. At a rate of $2/T$ ($40\ 000$ s^{-1} with $T = 50$ μs), only $\sim$14% of the information is stored, implying a correction for pileup losses of $\sim$7. One important point is evident: to maximize system throughput and minimize the necessary corrections, T must be minimized and some loss of resolution must always be accepted. Fortunately, much progress has been made in recent years to minimize T and still preserve resolution and peak shape (see Chapter 4 and Ref. 13).

If Equations 5-59 through 5-62 are used to estimate throughput rates and loss fractions, R and T must be reasonably well known. The input rate R is usually easy to obtain. Many modern amplifiers include a provision for pileup rejection and have a fast timing channel with a pulse-pair resolution of about 0.5 to 1.0 μs and an output that can be counted with a scaler-timer. Equation 5-56 can be used to refine the value of R when there is significant loss in the fast counting channel. Fast amplifiers and discriminators can be connected to the preamplifier output to measure the gross count rate. The SCA output on the ADC should not be used to measure R because it operates on the much slower amplifier output.

The rejection or loss interval T is more difficult to estimate. If electronic pileup rejection is not used, T can be assumed to be approximately equal to the pulse width (see Figure 5.13). An oscilloscope can be used to measure the width between the 1% or 2% amplitude points of the pulse. For many amplifiers, the pulse width is approximately six times the time constant τ, but this usually underestimates the pileup losses. After a pulse is analyzed, the amplifier output must fall below the ADC lower-level discriminator before another event is accepted. Because the discriminator level is usually low, a pulse preceded by another with less than a full pulse width separation will not be analyzed. To compensate, T might be estimated at about 1.5 times the pulse width for systems without formal pileup rejection.

With electronic pileup rejection, different configurations have somewhat different values of T. One common procedure uses a fast timing circuit to examine the intervals between preamplifier pulses and to generate an inhibit signal if an interval is less than a fixed value. The interval and inhibit signal length are approximately the width of an amplifier pulse. The inhibit signal is applied to the anticoincidence gate of the ADC to prevent analysis of pileup events. The value of T depends on the anticoincidence requirements of the ADC; usually a pulse is rejected if another pulse precedes it within the preset interval or if another pulse follows it before the ADC linear gate closes when digitization begins. Obviously, a good qualitative understanding of the operation of the ADC and pileup rejection circuitry is required to estimate T accurately. Additional losses caused by ADC deadtime can often be ignored. For example, if the pulse width is 35 μs (corresponding to use of ~6-μs time constants) and digitization takes 15 μs or less beginning when the pulse drops to 90% of its maximum value, then the ADC completes digitization and storage before the pileup inhibit signal is released and the ADC contributes no extra loss.

The fraction of good information stored is usually somewhat less than estimated. One reason is that rejection circuitry allows some pileup events to be analyzed, thus causing a loss of good events. Most pileup rejection circuitry has a pulse-pair resolution of 0.5 to 1.0 μs. Pulses separated by less than the resolution time will pile up but are still analyzed, causing sum peaks in the spectrum. When amplifier time constants of ≥ 3 μs are used, the pulse tops are nearly flat for a microsecond, and events within the resolving time of the pileup circuitry sum together almost perfectly, forming sum

peaks that have almost the same shape and width as real peaks. Such peaks are sometimes mistaken for single gamma-ray peaks and have a habit of appearing at embarrassing places in the spectrum.

Another cause of information loss is the generation of long-risetime preamplifier pulses. Usually preamplifier risetimes are a few tenths of a microsecond. However, if the gamma-ray interaction is in a part of the detector where the electric field is weak or where there is an excess of trapping centers, it may take several microseconds to collect the liberated charge. The main amplifier produces a very long, low-amplitude pulse, often two or three times as long as normal. Good events that sum with these long, low-amplitude pulses are lost as useful information. The frequency with which such events are generated depends on detector properties and how the detector is illuminated with gamma rays. Gamma rays falling on the detector edges where fields are often distorted and weak have a much greater chance of not being properly collected. In some applications, a detector performs better at high rates if the gamma rays can be collimated to fall only on its center region. For a relatively poor detector, under fully illuminated conditions, as many as 10% of the detected events can have long risetimes, and this results in a substantial loss of potential information. To achieve high throughput at high rates requires an excellent detector with minimum generation of the poorly collected, slow-rising pulses.

With appropriate sources and equipment, the throughput curve can be determined experimentally. Figure 5.15 shows the throughput curve for a state-of-the-art high-rate system employing time-variant filtering techniques (Chapter 4) to achieve very high throughput with almost constant resolution. A small planar germanium detector is used with a ^{241}Am source. The measured maximum throughput is $\sim$85 000 s^{-1} at an input rate of $\sim$300 000 s^{-1}. However, the paralyzable deadtime model predicts a maximum throughput of 110 000 s^{-1} with an input rate of 300 000 s^{-1}; the simple model is not adequate. The system resolution at 60 keV is almost constant at $\sim$0.63 keV up to an input rate of 100 000 counts/s and then increases smoothly to $\sim$0.72 keV at an input rate of 1 000 000 counts/s. Figure 5.16 shows the throughput curve for ^{241}Am using standard high-quality electronics optimized for high resolution at low count rates with 6-μs shaping constants and a 100-MHz Wilkinson ADC to generate an 8192-channel spectrum. Additional loss comes from resetting the pulsed-optical preamplifier. The maximum throughput of this system is only $\sim$2800 s^{-1}, but the resolution at 60 keV is $\sim$0.34 keV at the lowest rates and is still only $\sim$0.44 keV at 21 500 s^{-1}. The curves of throughput and resolution demonstrate that with the current state-of-the-art one cannot simultaneously obtain high throughput at a high rate and the best resolution. The FWHM increases by a factor of nearly 2 from the system optimized for resolution to that of the system optimized for high throughput. The two experimental curves, though describing very different systems, are similar to one another and to the theoretical curve shown in Figure 5.14 for the purely paralyzable system.
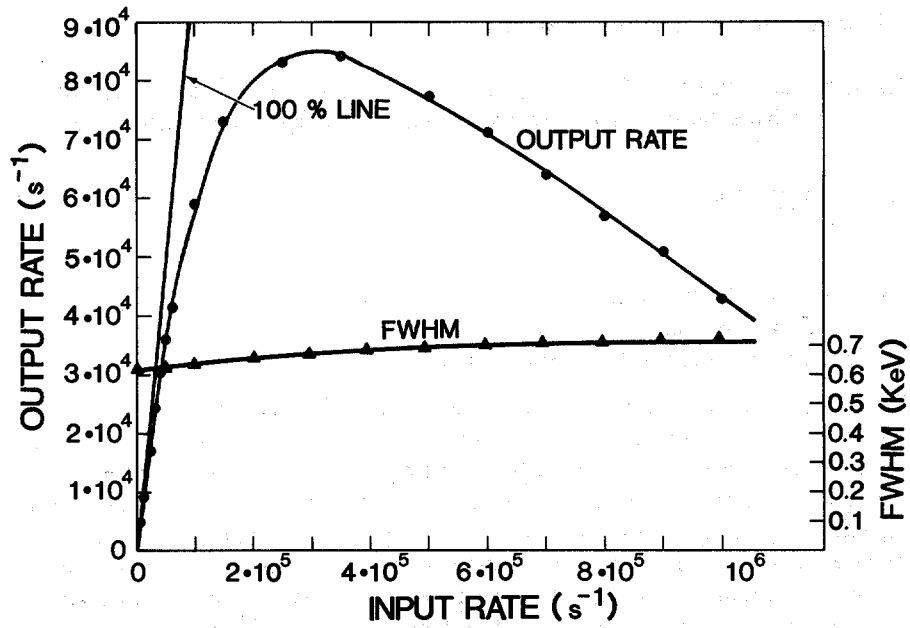
Fig. 5.15 *Experimental throughput and resolution curves for a state-of-the-art high-rate gamma-ray spectroscopy system. The straight line indicates 100% throughput.*
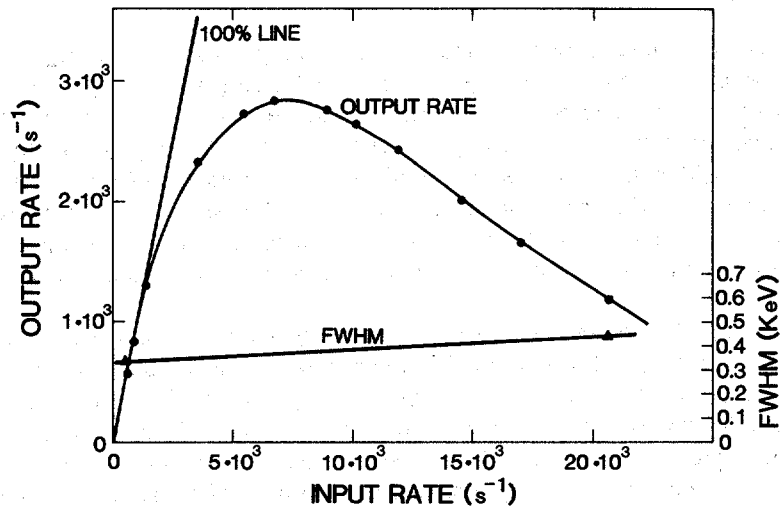

Fig. 5.16 *Experimental throughput and resolution curves for a standard gamma-ray spectroscopy system that is optimized for resolution at the expense of throughput. The line indicates 100% throughput.*

5.4.4 Correction Methods: General

The determination of the full-energy interaction rates (FEIR) of the gamma rays of interest is fundamental to many NDA procedures. The assayist must determine

$$\text{FEIR} = \frac{A(\gamma)}{TT}\text{CF(RL)} \qquad\qquad (5\text{-}63)$$

where $A(\gamma)$ = full-energy-peak area
          TT = true time of acquisition
   $CF(RL)$ = rate-related loss correction factor.

Three classes of correction procedures are discussed in this section. For detecting pileup events, the first procedure uses fast-timing electronics to measure the intervals between pulses. Corrections are made by extending the count time or by adding counts to the spectrum during acquisition. The second procedure adds an artificial peak to the spectrum by connecting a pulser to the preamplifier. The third procedure uses a gamma-ray source to generate the correction peak. The second and third procedures both use the variation in the correction-peak area to calculate a correction factor.

All three methods require the assumption that all peaks suffer the same fractional loss from the combined effects of pileup and deadtime; in general, the assumption is good.

5.4.5 Pileup Correction Methods: Electronic

Methods that extend count time employ fast counting circuits that operate directly from the preamplifier output; the time constants involved allow a pulse-pair resolution of 0.5 to 1.0 μs. The time resolution is achieved at the sacrifice of energy resolution so that some small pulses analyzed by the ADC are lost to the timing circuitry. The circuitry can neither detect nor correct for pileup events where the interval is less than the circuit resolving time or where one of the events is below the detection threshold. When two or more pulses are closer together than the chosen pileup rejection interval, the distorted event is not stored and the count time is extended to compensate for the loss.

One method of extending the count time is to generate a deadtime interval that begins when a pileup event is detected and ends when the next good event has been processed and stored; this procedure is approximately correct. The procedure cannot compensate for undetected events; however, with a typical rejection-gate period of 20 μs and a pulse-pair resolving time of $\sim$1 μs, the correction error may be only a few percent. For rates up to several tens of thousands of counts per second, the

total error may be only 1% or less; the necessary circuitry is frequently built into spectroscopy amplifiers. The method requires live-time operation, so the assay period is not known a priori. The method also requires that the count rate and spectral shape are constant during the counting period; this limitation is of no consequence for the assay of long-lived isotopes, but it is important in activation analysis of very short lived isotopes.

In recent years, the activation analysis requirement to handle high count rates and rapidly changing spectral shapes has led to further advancement in deadtime-pileup corrections. Such systems are complex and are just now becoming commercially available. They can handle input rates of hundreds of thousands of counts per second and accurately correct for losses in excess of 90%. The ability to correct for deadtime-pileup losses at high rates can potentially improve the speed of some NDA procedures.

5.4.6 Pulser-Based Corrections For Deadtime and Pileup

The pulser method uses a pulser to insert an artificial peak into the stored spectrum; it has numerous variations depending on the type of pulser used. Most germanium and silicon detector preamplifiers have a TEST input through which appropriately shaped pulses can be injected. These pulses suffer essentially the same deadtime and pileup losses as gamma-ray pulses and form a peak similar to a gamma-ray peak. The pulser peak has better resolution and shape than gamma-ray peaks because it is not broadened by the statistical processes involved in the gamma-ray detection process. The pulser peak area is determined in the same way as a gamma-ray peak area. The number of pulses injected into the preamplifier is easily determined by direct counting or by knowing the pulser rate and the acquisition time.

An advantage of the pulser method is that the artificial peak can usually be placed to avoid interference from gamma-ray peaks. In addition, because all the pulser events are full energy, minimum extra deadtime and pileup are generated. On the other hand, it is difficult to find pulsers with adequate amplitude stability, pulse-shaping capability, and rate flexibility.

Another common problem is the difficulty of injecting pulses through the preamplifier without some undershoot on the output pulse. A long undershoot is objectionable because gamma-ray pulses can pile up on the undershoot like they do on the positive part of the pulse. The amplifier pole zero cannot compensate simultaneously for the different decay constants of the pulser and gamma-ray pulses, and compensation networks are rarely used at the TEST input because of probable deterioration in resolution. The undershoot problem can be minimized by using a long decay time on the pulser pulse (often as long as a millisecond), by using shorter amplifier time constants, and by using high baseline-restorer settings. Some sacrifice of overall resolution is usually required to adequately minimize the undershoot problem.

The simplest approach is to use an ordinary fixed-period pulser, in which the interval between pulses is constant and equal to the reciprocal of the pulse rate. The best amplitude stability comes from the mercury-switch pulser in which a capacitor is charged and discharged through a resistor network by a mercury-wetted mechanical switch. The mechanical switch limits the useful rate of such pulsers to ≤ 100 Hz.

Assuming that the pulser peak and gamma-ray peaks lose the same fraction of events from deadtime and pileup, the appropriate correction factor is

$$CF(RL) = N/A(P) \tag{5-64}$$

where   N = number (rate) of pulses injected

A(P) = area (area rate) of pulser peak.

CF(RL) has a minimum value of 1.00 and is the reciprocal of the fraction of events stored in the peaks.

Equation 5-64 is not quite correct because pulser pulses are never lost as a result of their own deadtime, nor do they pileup on one another. Thus the overall losses from gamma-ray peaks are greater than those from the pulser peak although the difference is usually small. At moderate rates, the deadtime and pileup losses are nearly independent and CF(RL) can be corrected with two multiplicative factors to obtain a more accurate result:

$$CF(RL) = \frac{N}{A(P)}(1 + RT_D)(1 + RT) \tag{5-65}$$

where R = pulser rate

T_D = deadtime for pulser pulse

T = pileup interval.

The deadtime T_D can be adequately estimated from the speed of the ADC and, for Wilkinson ADCs, from the position of the pulser peak. The interval T is usually one and one-half to two times the pulse width. If R is ≤ 100 Hz, both factors are usually small. Assuming a typical value of 20 μs for both T_D and T, the value of each additional factor is 1.002 so that the increase in CF(RL) is only $\sim 0.4\%$. Larger corrections result if greater values of R, T_D, or T are used. If R is increased to 1000 Hz to obtain high precision more quickly, the additional factors make a difference of several percent.

Concern about assay precision brings up a rather curious but useful property of periodic pulsers. The precision of the pulser peak is given by a different relation than that of gamma-ray peaks. The precision of a pulser peak is, in fact, always better than the precision of a gamma-ray peak of the same area because gamma-ray emission

is random and the generation of pulser pulses is not. The precision of gamma-ray peak areas is governed by Poisson statistics whereas the precision of pulser peaks is governed mostly by binomial statistics.

Assuming that the background under the pulser peak is negligible and that the peak area is P, the variance and relative variance of P are given by

$$S^2(P) = P (1 - P/N)$$

$$S_r^2(P) = \frac{1}{P} (1 - P/N)$$

(5-66)

where N is the total number of pulses injected into the spectrum. Assuming again that the Compton continuum is negligible, the variance and relative variance of a gamma-ray peak of area A are given by

$$S^2(A) = A$$

$$S_r^2(A) = 1/A .$$

(5-67)

Figure 5.17 gives $S_r(P)$ versus P for several choices of P/N and demonstrates that by the time P/N $\approx$ 0.5 the improvement in precision is quite negligible.

When the pulser peak rests on a significant continuum, the expressions for S(P) are more complex because of the random nature of the continuum. The pulser peak
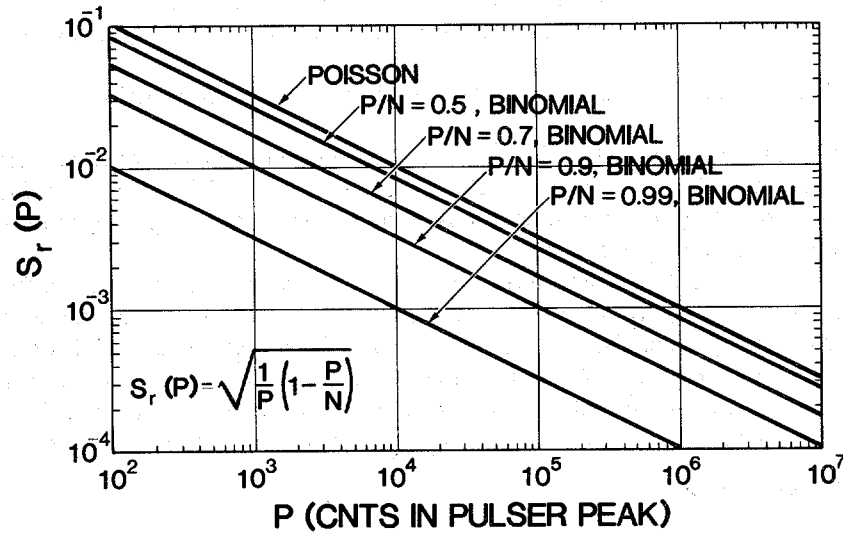

Fig. 5.17 *The relative standard deviation $S_r(P)$ of a pulser peak area P as a function of P for several values of P/N where N is the total number of pulses injected into the spectrum.*

should be placed in a low-continuum (usually high-energy) portion of the spectrum so that the improved precision can be taken advantage of and the simple Equation 5-66 can be used.

The use of a high-energy pulser peak can complicate the minimization of the undershoot. An alternative approach is to use a rectangular pulse that is longer than the amplifier output; then the pole-zero problem disappears and there are no shallow undershoots. Instead, a negative pulse is generated as the pulser output drops. Other events pile up on the negative pulse, but the pulse is cleanly defined and tends to throw pileup events out of their peak. The additional factor for the pileup losses can be written as (1 + 2RT).

If an adequate random pulser were available, CF(RL) would be given simply by Equation 5-64. Unfortunately, although random pulsers have been used successfully in research laboratories, no adequate unit is commercially available. It is difficult to simultaneously achieve the desired amplitude stability, random-interval distribution, and constant average rate required for routine gamma-ray assay applications.

Pulser-based deadtime-pileup corrections are accurate only when both rate and spectral shape are constant throughout the counting period. When the count rate changes during a measurement, proper corrections cannot be made if the pulser operates at a fixed rate. In principle, a correction can be made using a pulser that operates at a rate that is a fixed function of the gross detector rate. Pulsers based on this concept have been built and used successfully (Ref. 14). They are used in activation analysis, half-life studies, accelerator experiments, and anywhere that variable rates with constant spectral shape might be encountered. The use of variable rate pulsers indicates the variety and ingenuity with which the fundamental idea of inserting a synthetic peak into a spectrum has been applied to the problem of deadtime-pileup corrections.

5.4.7 Reference-Source Method for Deadtime-Pileup Corrections

The most accurate method for measuring the deadtime-pileup correction uses a reference source fixed in position relative to the detector. The source provides a constant gamma-ray interaction rate in the detector. The reference peak performs the same function as the pulser peak.

Like the other methods, the reference-source method requires the assumption that all peaks suffer the same fractional loss from deadtime and pileup. Given this assumption, the ratio of any peak area to the reference peak area is independent of such losses. Let $A(\gamma)$ and $FEIR(\gamma)$ represent, as usual, the full-energy-peak area and the full-energy interaction rate of any gamma ray other than the reference gamma ray R. If F is the common fraction stored and TT is the true acquisition time, then the areas are

$$A(\gamma) = F \times FEIR(\gamma) \times TT$$

$$A(R) = F \times FEIR(R) \times TT \ .$$

<div align="right">(5-68)</div>

The ratio of the two expressions gives

$$A(\gamma)/A(R) = FEIR(\gamma)/FEIR(R) \tag{5-69}$$

which is independent of both F and TT. Gamma-ray assays often are based directly on the loss-independent ratios $A(\gamma)/A(R)$ without ever explicitly determining CF(RL) or FEIR(γ).

For the reference-source gamma ray, the correction factor becomes

$$CF(RL) = FEIR(R) \times TT/A(R) . \tag{5-70}$$

Combining this expression with Equation 5-63 gives

$$FEIR(\gamma) = \frac{A(\gamma)}{A(R)} FEIR(R) \tag{5-71}$$

which is independent of count time. Equation 5-55 for the corrected count rate CR can now be rewritten

$$\begin{aligned} CR(\gamma) &= FEIR(\gamma) \times CF(AT) \\ &= \frac{A(\gamma)}{A(R)} FEIR(R) \times CF(AT) . \end{aligned} \tag{5-72}$$

The magnitude of CR(γ) does not depend on the true acquisition time although its precision obviously does.

If assay systems are calibrated with the help of standards, it is unnecessary to know FEIR(R) to obtain accurate assay values. In many assay procedures, the quantity sought, M (isotope or element mass), is proportional to CR(γ). In Equation 5-73 through 5-75, K is the calibration constant, the subscript s denotes quantities pertaining to standards, and the subscript u denotes quantities pertaining to unknowns.

$$M_u = \frac{CR(\gamma)_u}{K} = \frac{[A(\gamma)_u/A(R)_u]FEIR(R) \times CF(AT)_u}{K} \tag{5-73}$$

The calibration constant can be determined from a single standard:

$$K = \frac{CR(\gamma)_s}{M_s} = \frac{[A(\gamma)_s/A(R)_s]FEIR(R) \times CF(AT)_u}{M_s} \tag{5-74}$$

Combining Equations 5-73 and 5-74 gives

$$M_u = \frac{[A(\gamma)_u/A(R)_u]CF(AT)_u}{[A(\gamma)_s/A(R)_s]CF(AT)_s} M_s \tag{5-75}$$

which is independent of FEIR(R).

Although an accurate value of FEIR(R) is not needed, it is useful in obtaining approximate values of FEIR(γ), FEIR(R), and CF(RL) so that actual rates of data acquisition are known along with the fraction of information being lost to deadtime and pileup. Having a calibration constant expressed as corrected counts per second per unit mass can be helpful when estimating required assay times.

A reasonably accurate value of FEIR(R) can be obtained by making a live-time count of the reference source alone and estimating a correction for the pileup losses. A more accurate value can be obtained by using a pulser to correct for deadtime-pileup losses.

The reference-source method can be applied to any spectroscopy system without additional electronics. The method avoids problems caused by injecting pulser pulses into a preamplifier and by drift of the reference peak relative to the gamma-ray peaks. It also avoids the extra corrections required by a fixed-period pulser. Additionally, no error occurs because of the finite pulse-pair resolving time, and the reference peak is constantly present for digital stabilization and for checking system performance.

The most significant limitation to the procedure is that a reference source with appropriate half-life and energy is not always available. An additional limitation is that the reference source must have a significant count rate and this causes additional losses and results in poorer overall precision than that achievable using the same count time with other methods. The reference-source method, as well as the simpler pulser method, is only applicable when the count rate and spectral shape are constant.

The reference source should have a long half-life and an intense gamma ray in a clear portion of the spectrum. The energy of the reference gamma ray should be lower than but relatively close to the energy of the assay gamma rays so as not to add to the background beneath the assay peaks. A monoenergetic reference source limits the increase in gross count rate and overall deadtime-pileup losses. Few sources meet all the desired criteria, but several have proven adequate in many applications.

For ^{239}Pu assays based on the 413.7-keV gamma ray, ^{133}Ba is the most useful source. Its 356.0-keV gamma ray does not suffer interference from any plutonium or americium gamma ray and it is within 60 keV of the assay energy. The 10.3-yr half-life is very convenient. Although ^{133}Ba has several other gamma rays, they are all at energies below 414 keV.

For plutonium assays that make use of lower energy gamma rays, ^{109}Cd is a useful reference source. The 88.0-keV gamma ray is its only significant emission except for the $\sim$25-keV ^{109}Ag x rays from electron capture, which are easily eliminated by a thin filter. Its half-life of $\sim$453 days is adequate to give a year or two of use before replacement. Although no interfering gamma rays from plutonium or americium isotopes are present, there is a possible interference from lead x rays fluoresced in the detector shielding. The lead $K_{\beta 2}$ x ray falls almost directly under the 88.0-keV gamma ray from ^{109}Cd. Interference can be avoided by wrapping the detector in cadmium to absorb the lead x rays, and by using a sufficiently strong ^{109}Cd source that any residual leakage of lead x rays is overwhelmed. If some totally different

shielding material can be used (for example, iron or tungsten alloys), the problem disappears.

For assays of ^{235}U, the 122.0-keV gamma ray from ^{57}Co is used frequently. Its 271-day half-life is adequate, although not as long as might be desired. The 122.0-keV gamma ray is approximately eight times more intense than the 136.5-keV gamma ray, which is the only other gamma ray of significant intensity. Note that in using ^{57}Co for assay of highly enriched uranium samples, the 120.9-keV gamma ray from ^{234}U can be an annoying interference. This problem can be effectively eliminated by using a filter to reduce the intensity of lower energy emissions relative to the 185.7-keV intensity and a sufficiently strong ^{57}Co source to override any residual ^{234}U signal.

Frequently ^{241}Am can be used as a reference source for uranium or other assays. Although the 59.5-keV gamma ray from ^{241}Am is further removed from 186 keV than desirable, it can be used successfully, particularly if steps are taken to reduce the resolution difference. The half-life of 433.6 y is beyond fault. Americium-241 must be absolutely absent from any materials to be assayed. When using ^{169}Yb as a transmission source in densitometry or quantitative ^{235}U assay, ytterbium daughters emit x rays that directly interfere with the 59.5-keV gamma ray, but sufficient filtering combined with adequate source intensity can eliminate any possible difficulty.

The current methods for deadtime-pileup correction assume that all full-energy peaks suffer the same fractional loss. That assumption is not completely true primarily because the width and detailed peak shape are functions of both energy and count rate. In applying the reference-peak method, precautions can be taken to minimize the degree to which the assumption falls short. Four of those precautions, most of which apply to any of the correction methods, are listed below.

- Where possible, apply the procedure only over a narrow energy range.
- Keep the peak width and shape as constant as possible as functions of both energy and count rate, even if that slightly degrades the low-rate and low-energy resolution. Proper adjustment of the amplifier and the pileup rejection can help considerably.
- Avoid a convex or concave Compton continuum beneath important peaks, especially the reference peak. If possible the ratio of the reference peak area to the background area should be ≥ 10.
- Exercise great care in determining peak areas. ROI methods may be less sensitive than some of the spectral fitting codes to small changes in peak shape.

Experimental results indicate that the reference-source method can correct for deadtime and pileup losses with accuracies approaching 0.1% over a wide count-rate range. Such accuracies can also be approached by pulser methods, particularly at lower rates and by some purely electronic methods. However, equipment for the purely electronic methods is very sophisticated.

5.5 EFFECTS OF THE INVERSE-SQUARE LAW

The absolute full-energy detector efficiency varies approximately as the inverse square of the distance between the detector and gamma-ray source. Consider a point source emitting I gamma rays per second. The gamma-ray flux F at a distance R is defined as the number of gamma rays per second passing through a unit area on a sphere of radius R centered at the source. Because the area of the sphere is $4\pi R^2$, the expression for F is

$$F = \frac{I}{4\pi R^2} \cdot \qquad\qquad (5\text{-}76)$$

The detector count rate is proportional to the incident flux, and if the detector face can be approximated by a portion of a spherical surface centered at the source, the count rate has the same $1/R^2$ dependency as the flux. When low-intensity samples are counted, there is a clear motivation to reduce the sample-to-detector distance and increase the count rate. Unfortunately, when the sample-to-detector distance is so small that different parts of the sample have significantly different distances to the detector, the count rates from different parts of the sample vary significantly. This variation can cause an assay error when the distribution of emitting material is nonuniform.

The overall count rate from samples of finite extent does not follow the simple law; usually the variation is less strong than $1/R^2$. Knowledge of a few simple cases can help to estimate overall count rates and response uniformity.

The simplest extended source is a line, which is often an adequate model of a pipe carrying radioactive solutions. Consider an ideal point detector with intrinsic efficiency ε at a distance D from an infinitely long source of intensity I per unit length (Figure 5.18). The count rate from this source can be expressed as

$$CR = 2\int_0^\infty \frac{I\varepsilon\ dr}{r^2 + D^2} = \frac{\pi I\varepsilon}{D} \cdot \qquad\qquad (5\text{-}77)$$

In this ideal case, the count-rate dependence is $1/R$ rather than $1/R^2$; when pipes are counted at distances much smaller than their length, the count-rate variation will be approximately $1/R$.

The count rate from a point detector at a distance R from an infinite plane surface does not depend on R at all. For a detector near a uniformly contaminated glovebox wall, count rates vary little with wall-to-detector distance changes.

When possible the variation of response with position inside a sample should be minimized. The sample-to-detector distance can be increased, but the penalty is a severe loss of count rate. A better strategy is to rotate the sample. Consider the cross section of a cylindrical sample of radius R whose center is at a distance D from a detector (Figure 5.19). Unless D is much greater than R, the count rates for identical sources at positions 1, 2, 3, and 4 vary considerably. The figure shows that if D = 3R, the maximum count-rate ratio is CR(2)/CR(4) = 4. The ratio of the response of a rotating source at radius R to the response at the center (position 1 of Figure 5.19) is

$$\frac{CR(R)}{CR(1)} = \frac{1}{1 + (R/D)^2} \, . \tag{5-78}$$

The response is the same as that obtained for a uniform nonattenuating circular source of radius R whose center is at a distance D from a detector. Table 5-6 gives the value of this function for several values of R/D compared to CR(2)/CR(1) for the nonrotating source of Figure 5.19. For relatively large values of R/D, rotation improves the uniformity of response. The response variation is even larger when attenuation is considered. Rotation only reduces $1/R^2$ effects; it does not eliminate them completely.
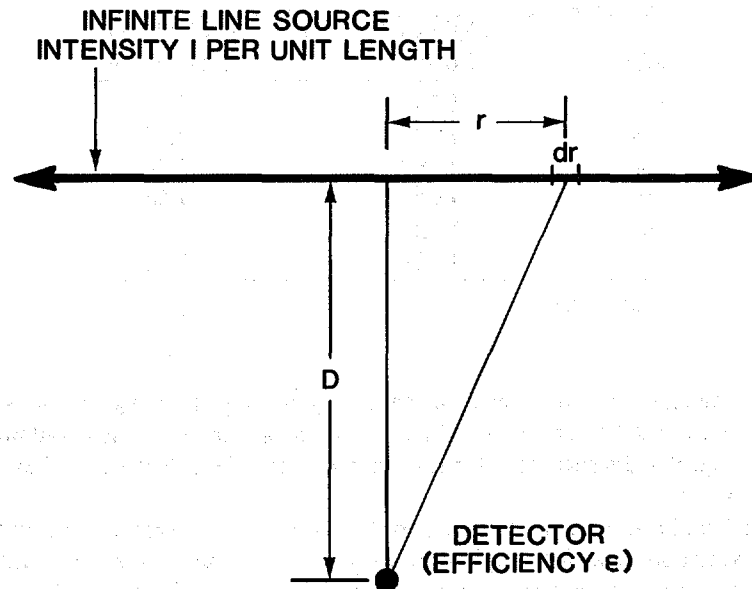

INFINITE LINE SOURCE
INTENSITY I PER UNIT LENGTH

DETECTOR
(EFFICIENCY ε)

Fig. 5.18 Geometry for computing the response of a point detector to a line source.

CR (2)/CR (1) = 2.25
CR (3)/CR (1) = 0.90
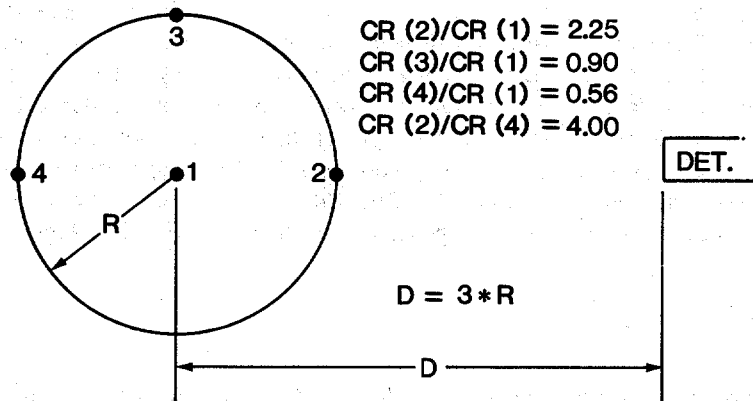CR (4)/CR (1) = 0.56
CR (2)/CR (4) = 4.00

DET.

$D = 3*R$

D

Fig. 5.19 *Cross section through a cylindrical sample and a point detector showing how count rate varies with position.*

Table 5-6. The effect of sample rotation on count-rate variation

R/D	CR(R)/CR(1) (Rotating)	CR(2)/CR(1) (Nonrotating)
1/2	1.33	4.0
1/3[a]	1.125	2.25
1/4	1.067	1.78
1/5	1.042	1.56
1/6	1.029	1.44
1/7	1.021	1.36

[a]See Figure 5.19.

Rotation reduces response variations caused by radial positioning, but does little to compensate for height variations. If the source height is less than one-third of the sample-to-detector distance, the decrease in response is less than 10% relative to the normal position.

The choice of sample-to-detector distance is a compromise between minimizing the response variations and maintaining an adequate count rate. A useful guideline is that the maximum count-rate variation is less than ±10% if the sample-to-detector distance is equal to three times the larger of the sample radius or the half-height. If a sample cannot be rotated, it helps considerably to count it in two positions 180° apart.

5.6 DETECTOR EFFICIENCY MEASUREMENTS

5.6.1 Absolute Full-Energy-Peak Efficiency

The absolute full-energy-peak efficiency is the fraction of gamma rays emitted by a point source at a particular source-to-detector distance that produces a full-energy interaction in the detector. It is determined as a function of energy by measuring the efficiency at a number of energies and fitting the experimental points with an appropriate function:

$$\varepsilon_A(\gamma) = \text{FEIR}(\gamma)/\text{ER}(\gamma) \tag{5-79}$$

where ε_A = absolute full-energy efficiency
$\text{ER}(\gamma)$ = gamma-ray emission rate.

The determination of FEIR is described in Section 5.4. For high-resolution detectors, care must be taken to correct for pileup and deadtime losses. For low-resolution scintillators, the pileup correction can usually be ignored.

Calibrated sources for absolute calibrations are available from a number of vendors. It is a testimony to the difficulty of measuring accurate emission rates that the quoted accuracies are only between 0.5% and 2.0%. Table 5-1 lists several monoenergetic gamma-ray sources. Multi-isotope, multi-gamma-ray sources, such as the NBS source SRM-4275 (see Section 5.1.1), are convenient when calibrating high-resolution detectors. This source is useful for several years and covers the energy range most often of use in NDA.

Frequently two or more gamma rays are emitted in successive transitions between energy levels of a single excited nucleus. Because the time interval between such cascade gamma rays is very small compared to the charge collection times of germanium, silicon, or NaI(Tl) detectors, the multiple gamma rays are treated as a single interaction. This cascade summing can result in subtractive or additive errors in the measured FEIRs. The problem is significant when the source is so close to the detector that the probability of detecting two or more cascade gamma rays simultaneously is large. If very short source-to-detector distances must be used to enhance sensitivity, cascade-summing problems must be carefully considered. The notes accompanying SRM-4275 contain a good discussion of summing problems as well as other possible difficulties involved in the use of multi-gamma-ray sources.

5.6.2 Intrinsic Full-Energy Efficiency

The intrinsic full-energy efficiency is the probability that a gamma ray loses all of its energy if it enters the detector volume. The absolute full-energy efficiency ε_A and the intrinsic full-energy efficiency ε_I are related by the simple equation

$$\varepsilon_A = \frac{\Omega}{4\pi} \varepsilon_I \tag{5-80}$$

where Ω is the solid angle subtended by the detector at the source and $\Omega/4\pi$ is the probability that a gamma ray will enter the detector volume. The intrinsic full-energy efficiency is determined experimentally by measuring the absolute full-energy efficiency and solving Equation 5-80 for ε_I. The values of ε_I computed will depend slightly upon the position of the source with respect to the detector.

Some care is necessary in estimating the solid angle Ω, especially if the detector has an odd shape or is not located on an axis of symmetry. Figure 5.20 shows a point source at a distance D from the face of a cylindrical detector of radius R. The correct expression for the solid angle subtended by the detector at the source is

$$\Omega = 2\pi \left[1 - \left(\frac{D}{\sqrt{D^2 + R^2}} \right) \right] \tag{5-81}$$

where $D/\sqrt{D^2 + R^2} = \text{Cos } \Theta$, with Θ being the angle of the solid-angle cone shown in Figure 5.20. However, for a circular detector, an approximate expression is frequently used:

$$\Omega \approx A/D^2 = \pi R^2/D^2 \tag{5-82}$$

where A is the area of the detector face. The first expression in Equation 5-82 can be applied even when the detector is not circular, but is only accurate when A is much less than $4\pi D^2$. Comparing Equations 5-81 and 5-82 shows that as D decreases relative to R, the value for Ω from Equation 5-82 becomes too large. For D/R = 8, Ω is ~1% too large; for D/R = 1, Ω is ~70% too large.
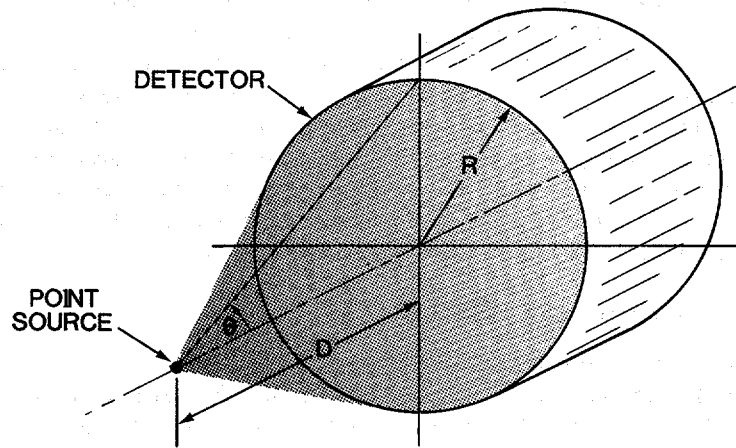

Fig. 5.20 A point source on the axis of a cylindrical detector.

5.6.3 Relative Efficiency

Frequently the actual values of the absolute or intrinsic full-energy-peak efficiency are not needed, and only the ratios of the efficiency at different energies are required. A relative efficiency curve is usually easier to determine than absolute or intrinsic efficiencies. Relative efficiencies differ from absolute or intrinsic efficiencies only by a multiplicative constant that depends upon the procedure used in determining the relative efficiencies. Exact gamma-ray emission rates are not required, only values proportional to the emission rates. When a single multienergy isotope is used, the branching fractions provide the necessary information (Ref. 15). Equation 5-79 can be modified to give relative efficiencies for a single source:

$$\varepsilon_R = A(\gamma)/B(\gamma) \tag{5-83}$$

where $B(\gamma)$ is the branching ratio corresponding to the peak area $A(\gamma)$. Usually relative-efficiency curves are normalized to 1.00 at some convenient energy. A semilog plot of relative efficiency has the same shape as the corresponding absolute-efficiency or intrinsic-efficiency plot. Figure 5.21 shows the relative-efficiency of a coaxial detector as derived from a single spectrum of a thin [133]Ba source. Note that sources with negligible self-attenuation must be used when the branching fractions are assumed to be proportional to the rates of gamma rays escaping from the source. This assumption is not true for many steel-encapsulated sources particularly at lower energies.
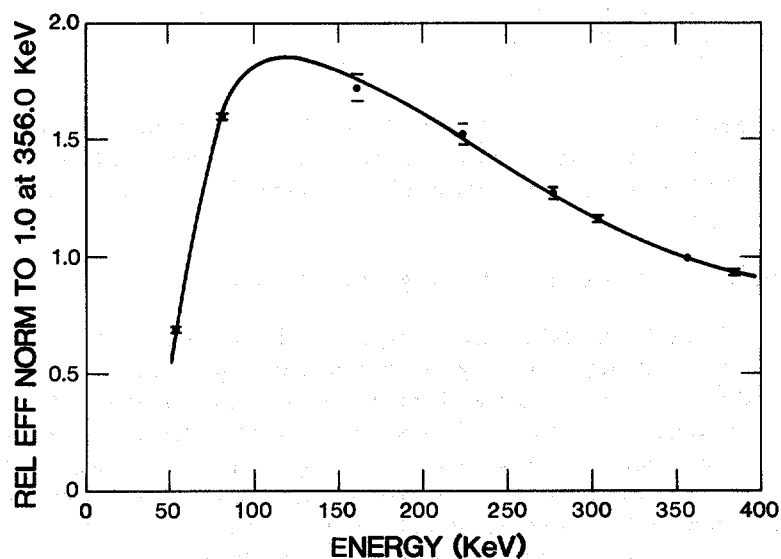

Fig. 5.21 Relative efficiency of a 30%-efficient coaxial germanium detector between ~50 and ~400 keV, as derived from a single spectrum of a thin [133]Ba source.

5.6.4 Efficiency Relative to a 7.65-cm by 7.65-cm NaI(Tl) Detector

The manufacturers of germanium detectors usually characterize the efficiency of coaxial detectors by comparing it to the absolute full-energy efficiency of a 7.65-cm by 7.65-cm NaI(Tl) detector. The comparison is always made at 1332.5 keV with a source-to-detector distance of 25.0 cm and the efficiency expressed as a percentage of the NaI(Tl) efficiency. The efficiency of the germanium detector is measured and the absolute full-energy efficiency of the NaI(Tl) detector is assumed to be 0.0012 for the stated energy and distance. The expression for computing the measured germanium-detector efficiency is

$$\varepsilon_{RNaI} = \left[\frac{FEIR(1332.5)/ER(1332.5)}{0.0012} \right] 100 \tag{5-84}$$

where FEIR(1332.5) includes corrections for deadtime-pileup losses and ER(1332.5) is the current emission rate. The source-to-detector distance is very difficult to determine accurately because the detector crystal is hidden inside the cryostat end cap. Because the front face of the detector crystal is mounted within 5 mm of the end cap by most manufacturers, the measurement is made at a source-to-end-cap distance of 24.5 cm.

If a 60-Hz pulser is used for the rate-related losses, Equation 5-84 can be rewritten as

$$\varepsilon_{RNaI} = \frac{135.1 \, A(1332.5)}{A(p)I_0 \, \exp(-0.1318T)} \tag{5-85}$$

where A(1332.5) and A(p) are the areas of the 1332.5-keV and pulser peaks, and where T is the time in years since the ^{60}Co source had an activity of I_0 microcuries. If the same ^{60}Co source is used consistently, the value of I_0 can be absorbed in the numerical constant.

5.6.5 Efficiency as Function of Energy and Position

Usually NDA calibrations are done using standards that contain known amounts of the isotopes of interest in packages of appropriate shape and size. Because approximate detector efficiencies are used only to estimate expected count rates, there is little need to carefully characterize efficiency as a function of energy and position. A detector so characterized can assay without the use of standards, although generally not with the same ease and accuracy as possible with them. When standards are not available or allowed in an area, verification measurements can be made of items of known geometry and content using the known detector efficiency to predict the FEIRs for a chosen detector-sample configuration. If the measured FEIRs agree within the estimated error with the predicted rates, the item content is regarded as verified.

In constructing appropriate efficiency functions, the absolute efficiency is measured for many energies and positions and then fit to an adequate mathematical model. Cline's method (Ref. 16) combines reasonable accuracy with a straightforward procedure for determining the efficiency parameters. To characterize a detector accurately takes several days or more.

REFERENCES

1. R. Gunnink, J. E. Evans, and A. L. Prindle, "A Reevaluation of the Gamma-Ray Energies and Absolute Branching Intensities of ^{237}U, ^{283,239,240,241}Pu, and ^{241}Am," Lawrence Livermore Laboratory report UCRL-52139 (1976).

2. M. E. Anderson and J. F. Lemming, "Selected Measurement Data for Plutonium and Uranium," Mound Laboratory report MLM-3009 (1982).

3. *Table of Isotopes*, 7th ed., C. M. Lederer and V. S. Shirley, Eds. (John Wiley & Sons, Inc., New York, 1978).

4. R. D. Evans, *The Atomic Nucleus* (McGraw-Hill Book Co., New York, 1955), Chapters 23–25.

5. P. R. Bevington, *Data Reduction and Error Analysis for the Physical Sciences* (McGraw-Hill Book Co., New York, 1969).

6. Y. Beers, *Introduction to the Theory of Error* (Addison-Wesley Publishing Co., Inc., Reading, Massachusetts, 1962).

7. T. Mukoyama, "Fitting of Gaussian to Peaks by Non-Iterative Method," *Nuclear Instrument and Methods* 125, 289–291 (1975).

8. S. L. Meyer, *Data Analysis for Scientists and Engineers* (John Wiley & Sons, Inc., New York, 1975), p. 37.

9. R. B. Walton, E. I. Whitted, and R. A. Forster, "Gamma-Ray Assay of Low-Enriched Uranium Waste," *Nuclear Technology* 24, 81–92 (1974).

10. R. Gunnink, "Computer Techniques for Analysis of Gamma-Ray Spectra," Lawrence Livermore Laboratory report UCRL-80297 (1978).

11. R. G. Helmer and M. A. Lee, "Analytical Functions for Fitting Peaks From Ge Semiconductor Detectors," *Nuclear Instruments and Methods* 178, 499–512 (1980).

12. G. K. Knoll, *Radiation Detection and Measurement* (John Wiley & Sons, Inc., New York, 1979).

13. J. G. Fleissner, C. P. Oertel, and A. G. Garrett, "A High Count Rate Gamma-Ray Spectrometer System for Plutonium Isotopic Measurements," *Journal of the Institute of Nuclear Materials Management* 14, 45–56 (1986).

14. H. H. Bolotin, M. G. Strauss, and D. A. McClure, "Simple Technique for Precise Determination of Counting Losses in Nuclear Pulse Processing Systems," *Nuclear Instruments and Methods* 83 1–12 (1970).

15. R. A. Meyer, "Multigamma-Ray Calibration Sources," Lawrence Livermore Laboratory report M-100 (1978).

16. J. E. Cline, "A Technique of Gamma-Ray Detector Absolute Efficiency Calibration for Extended Sources," Proc. American Nuclear Society Topical Conference on Computers in Activation Analysis and Gamma-Ray Spectroscopy, Mayaguez, Puerto Rico (1978), pp. 185–196 (Conf. 780421).